

An Open Pediatric Brain Tumor Atlas

This manuscript ([permalink](#)) was automatically generated from [AlexsLemonade/OpenPBTA-manuscript@41a7cc2](#) on August 24, 2021.

Authors

- **Joshua A. Shapiro**
 [0000-0002-6224-0347](#) ·  [jashapiro](#) ·  [jashapiro](#)
Childhood Cancer Data Lab, Alex's Lemonade Stand Foundation, Philadelphia, PA, USA · Funded by Alex's Lemonade Stand Foundation Childhood Cancer Data Lab (CCDL)
- **Candace L. Savonen**
 [0000-0001-6331-7070](#) ·  [cansavvy](#) ·  [cansavvy](#)
Childhood Cancer Data Lab, Alex's Lemonade Stand Foundation, Philadelphia, PA, USA · Funded by Alex's Lemonade Stand Foundation Childhood Cancer Data Lab (CCDL)
- **Chante J. Bethell**
 [0000-0001-9653-8128](#) ·  [cbethell](#) ·  [cjbethell](#)
Childhood Cancer Data Lab, Alex's Lemonade Stand Foundation, Philadelphia, PA, USA · Funded by Alex's Lemonade Stand Foundation Childhood Cancer Data Lab (CCDL)
- **Krutika S. Gaonkar**
 [0000-0003-0838-2405](#) ·  [kgaonkar6](#) ·  [29aprilkrutika](#)
Center for Data-Driven Discovery, Children's Hospital of Philadelphia; Division of Neurosurgery, Children's Hospital of Philadelphia; Department of Bioinformatics and Health Informatics, Children's Hospital of Philadelphia
- **Yuankun Zhu**
 [0000-0002-2455-9525](#) ·  [yuankunzhu](#) ·  [zhuyuankun](#)
Center for Data-Driven Discovery, Children's Hospital of Philadelphia; Division of Neurosurgery, Children's Hospital of Philadelphia
- **Miguel A. Brown**
 [0000-0001-6782-1442](#) ·  [migbro](#) ·  [migbro](#)
Center for Data-Driven Discovery, Children's Hospital of Philadelphia; Division of Neurosurgery, Children's Hospital of Philadelphia
- **Nhat Duong**
 [0000-0003-2852-4263](#) ·  [fingerfen](#) ·  [asiannhat](#)
Department of Bioinformatics and Health Informatics, Children's Hospital of Philadelphia
- **Komal S. Rathi**
 [0000-0001-5534-6904](#) ·  [komalsrathi](#) ·  [komalsrathi](#)
Center for Data-Driven Discovery, Children's Hospital of Philadelphia; Department of Bioinformatics and Health Informatics, Children's Hospital of Philadelphia
- **Nighat Noureen**
 [0000-0001-7495-8201](#) ·  [NNoureen](#)
Greehey Children's Cancer Research Institute, UT Health San Antonio
- **Bo Zhang**
 [0000-0002-0743-5379](#) ·  [zhangb1](#)

Center for Data-Driven Discovery, Children's Hospital of Philadelphia; Division of Neurosurgery, Children's Hospital of Philadelphia

- **Brian M. Ennis**

 [0000-0002-2653-5009](#) ·  [bmennis](#)

Center for Data-Driven Discovery, Children's Hospital of Philadelphia; Division of Neurosurgery, Children's Hospital of Philadelphia

- **Stephanie J. Spielman**

 [0000-0002-9090-4788](#) ·  [sjspielman](#) ·  [stephspiel](#)

Rowan University, Glassboro, NJ, USA · Funded by Alex's Lemonade Stand Foundation Childhood Cancer Data Lab (CCDL)

- **Bailey Farrow**

 [0000-0001-6727-6333](#) ·  [baileyckelly](#)

Center for Data-Driven Discovery, Children's Hospital of Philadelphia; Division of Neurosurgery, Children's Hospital of Philadelphia

- **Nicolas Van Kuren**

 [0000-0002-7414-9516](#) ·  [nicholasvk](#)

Center for Data-Driven Discovery, Children's Hospital of Philadelphia; Division of Neurosurgery, Children's Hospital of Philadelphia

- **Tejaswi Koganti**

 [0000-0002-7733-6480](#) ·  [tkoganti](#)

Center for Data-Driven Discovery, Children's Hospital of Philadelphia; Division of Neurosurgery, Children's Hospital of Philadelphia

- **Shrivats Kannan**

 [0000-0002-1460-920X](#) ·  [shrivatsk](#) ·  [kshrivats](#)

Center for Data-Driven Discovery, Children's Hospital of Philadelphia; Division of Neurosurgery, Children's Hospital of Philadelphia

- **Pichai Raman**

 [0000-0001-6948-2157](#) ·  [pichairaman](#) ·  [PichaiRaman](#)

Center for Data-Driven Discovery, Children's Hospital of Philadelphia; Department of Bioinformatics and Health Informatics, Children's Hospital of Philadelphia

- **Jennifer Mason**

·  [jenn0307](#) ·  [jenn0307](#)

Center for Data-Driven Discovery, Children's Hospital of Philadelphia; Division of Neurosurgery, Children's Hospital of Philadelphia

- **Daniel P. Miller**

 [0000-0002-2032-4358](#) ·  [dmiller15](#)

Center for Data-Driven Discovery, Children's Hospital of Philadelphia; Division of Neurosurgery, Children's Hospital of Philadelphia

- **Anna R. Poetsch**

 [0000-0003-3056-4360](#) ·  [arpoe](#) ·  [APoetsch](#)

Biotechnology Center, Technical University Dresden, Germany; National Center for Tumor Diseases, Dresden, Germany

- **Payal Jain**
 [0000-0002-5914-9083](#) ·  [jainpayal022](#) ·  [jainpayal022](#)
Center for Data-Driven Discovery, Children's Hospital of Philadelphia; Division of Neurosurgery, Children's Hospital of Philadelphia
- **Adam A. Kraya**
 [0000-0002-8526-5694](#) ·  [aadamk](#)
Center for Data-Driven Discovery, Children's Hospital of Philadelphia; Division of Neurosurgery, Children's Hospital of Philadelphia
- **Allison P. Heath**
 [0000-0002-2583-9668](#) ·  [allisonheath](#) ·  [allig8r](#)
Center for Data-Driven Discovery, Children's Hospital of Philadelphia; Division of Neurosurgery, Children's Hospital of Philadelphia
- **Mateusz P. Koptyra**
 [0000-0002-3857-6633](#) ·  [mkoptyra](#) ·  [koptyram](#)
Center for Data-Driven Discovery, Children's Hospital of Philadelphia; Division of Neurosurgery, Children's Hospital of Philadelphia
- **Yiran Guo**
 [0000-0002-6549-8589](#) ·  [Yiran-Guo](#) ·  [YiranGuo3](#)
Center for Data-Driven Discovery, Children's Hospital of Philadelphia; Division of Neurosurgery, Children's Hospital of Philadelphia
- **Xiaoyan Huang**
 [0000-0001-7267-4512](#) ·  [HuangXiaoyan0106](#)
Center for Data-Driven Discovery, Children's Hospital of Philadelphia; Division of Neurosurgery, Children's Hospital of Philadelphia
- **Jessica Wong**
 [0000-0003-1508-7631](#) ·  [wongjessica93](#) ·  [jessicawongbfx](#)
Center for Data-Driven Discovery, Children's Hospital of Philadelphia; Division of Neurosurgery, Children's Hospital of Philadelphia
- **Mariarita Santi**
 [0000-0002-6728-3450](#)
Department of Pathology and Laboratory Medicine, Children's Hospital of Philadelphia; Department of Pathology and Laboratory Medicine, University of Pennsylvania Perelman School of Medicine
- **Angela Viaene**
 [0000-0001-6430-8360](#)
Department of Pathology and Laboratory Medicine, Children's Hospital of Philadelphia; Department of Pathology and Laboratory Medicine, University of Pennsylvania Perelman School of Medicine
- **Laura Scolaro**

Division of Oncology, Children's Hospital of Philadelphia, Children's Hospital of Philadelphia
- **Angela Waanders**
 [0000-0002-0571-2889](#) ·  [awaanders](#)
Department of Oncology, Ann & Robert H. Lurie Children's Hospital of Chicago; Department of Pediatrics, Northwestern University Feinberg School of Medicine

- **Derek Hanson**
 [0000-0002-0024-5142](#)
Hackensack Meridian School of Medicine; Hackensack University Medical Center
- **Hongbo M. Xie**
 [0000-0003-2223-0029](#) ·  [xiehongbo](#) ·  [xiehb](#)
Department of Bioinformatics and Health Informatics, Children's Hospital of Philadelphia
- **Siyuan Zheng**
 [0000-0002-1031-9424](#) ·  [syzheng](#) ·  [zhengsiyuan](#)
Greehey Children's Cancer Research Institute, UT Health San Antonio
- **Cassie N. Kline**
 [0000-0001-7765-7690](#) ·  [cnkline13](#)
Division of Oncology, Children's Hospital of Philadelphia
- **Jena V. Lilly**
 [0000-0003-1439-6045](#) ·  [jvlilly](#) ·  [jvlilly](#)
Center for Data-Driven Discovery, Children's Hospital of Philadelphia; Division of Neurosurgery, Children's Hospital of Philadelphia
- **Philip B. Storm**
 [0000-0002-7964-2449](#)
Center for Data-Driven Discovery, Children's Hospital of Philadelphia; Division of Neurosurgery, Children's Hospital of Philadelphia
- **Adam C. Resnick**
 [0000-0003-0436-4189](#) ·  [adamcresnick](#) ·  [adamcresnick](#)
Center for Data-Driven Discovery, Children's Hospital of Philadelphia; Division of Neurosurgery, Children's Hospital of Philadelphia · Funded by Alex's Lemonade Stand Foundation; Children's Brain Tumor Tissue Consortium; NIH R01NS091620-05, 5U2CHL138346-04, 1U2CCA233285-03, 1OT2OD027852-01, 1OT3HL147154-01
- **Jo Lynne Rokita**
 [0000-0003-2171-3627](#) ·  [jharenza](#) ·  [jolynnerokita](#)
Center for Data-Driven Discovery, Children's Hospital of Philadelphia; Division of Neurosurgery, Children's Hospital of Philadelphia; Department of Bioinformatics and Health Informatics, Children's Hospital of Philadelphia · Funded by Alex's Lemonade Stand Foundation
- **Casey S. Greene**
 [0000-0001-8713-9213](#) ·  [cgreene](#) ·  [greenescientist](#)
Department of Systems Pharmacology and Translational Therapeutics, Perelman School of Medicine, University of Pennsylvania, Philadelphia, PA, USA; Childhood Cancer Data Lab, Alex's Lemonade Stand Foundation, Philadelphia, PA, USA · Funded by Alex's Lemonade Stand Foundation Childhood Cancer Data Lab (CCDL)
- **Jaclyn N. Taroni**
 [0000-0003-4734-4508](#) ·  [jaclyn-taroni](#) ·  [jaclyn_taroni](#)
Childhood Cancer Data Lab, Alex's Lemonade Stand Foundation, Philadelphia, PA, USA · Funded by Alex's Lemonade Stand Foundation Childhood Cancer Data Lab (CCDL)
- **Children's Brain Tumor Tissue Consortium**

- Pacific Pediatric Neurooncology Consortium

Abstract

Introduction

Introduction will go here.

Materials and Methods

Biospecimen collection

The Pediatric Brain Tumor Atlas specimens are comprised of samples from Children's Brain Tumor Network (CBTN) and the Pediatric Pacific Neuro-oncology Consortium (PNOC).

Children's Brain Tumor Tissue Consortium (CBTN)

The CBTN [1] is a collaborative, multi-institutional (18 institutions worldwide) research program dedicated to the study of childhood brain tumors. All CBTN data can be download from the Gabriella Miller Kids First Data Resource Center, [2]. The de-identified patient's blood and tumor tissue were prospectively collected by the consortium from patients enrolled within the CBTN.

The cell lines were generated by the CBTN from either fresh tumor tissue obtained directly from surgery performed at Children's Hospital of Philadelphia (CHOP) or from prospectively collected tumor specimens stored in Recover Cell Culture Freezing media (cat# 12648010, Gibco). The tissue was dissociated using enzymatic method with papain as described [3]. Briefly, tissue was washed with HBSS (cat# 14175095, Gibco), minced and incubated with activated papain solution (cat# LS003124, SciQuest) for up to 45 minutes. The papain was inactivated using ovomucoid solution (cat# 542000, SciQuest), tissue was briefly treated with DNase (cat# 10104159001, Sigma) and passed through the 100 μ m cell strainer (cat# 542000, Greiner Bio-One). Two cell culture conditions were initiated based on the number of cells available. For cultures utilizing the fetal bovine serum (FBS), a minimum density of 3 \times 10 5 cells/ml were plated in DMEM/F-12 medium (cat# D8062, Sigma) supplemented with 20% FBS (cat# SH30910.03, Hyclone), 1% GlutaMAX (cat# 35050061, Gibco), Penicillin/Streptomycin-Amphotericin B Mixture (cat# 17-745E, Lonza) and 0.2% Normocin (cat# ant-nr-2, Invivogen). For the serum-free media conditions cells were plated at minimum density of 1 \times 10 6 cells/ml in DMEM/F12 media supplemented with 1% GlutaMAX, 1x B-27 supplement minus vitamin A (cat# 12587-010, Gibco), 1x N-2 supplement (cat# 17502001, Gibco), 20 ng/ml epidermal growth factor (cat# PHG0311L, Gibco), 20 ng/ml basic fibroblast growth factor (cat# 100-18B, PeproTech), 2.5 μ g/ml heparin (cat# H3149, Sigma), Penicillin/Streptomycin-Amphotericin B Mixture and 0.2% Normocin.

Pacific Pediatric Neuro-oncology Consortium (PNOC)

The Pacific Pediatric Neuro-Oncology Consortium (PNOC) [4] is an international consortium dedicated to bringing new therapies to children and young adults with brain tumors. PNOC collected blood and tumor biospecimens from newly-diagnosed diffuse intrinsic pontine glioma (DIPG) patients as part of the clinical trial [PNOC003/NCT02274987](#) [5].

Nucleic acids extraction and library preparation

PNOC samples

The Translational Genomic Research Institute (TGEN; Phoenix, AZ) performed DNA and RNA extractions on tumor biopsies using a DNA/RNA AllPrep Kit (Qiagen, #80204). All RNA used for library prep had a minimum RIN of 7 but no QC thresholds were implemented for the DNA. For library preparation, 500ng of nucleic acids were used as input for RNA-Seq, WXS, and targeted DNA panel (panel). The RNA prep was performed using the TruSeq RNA Sample Prep Kit (Illumina, #FC-122-1001) and the exome prep was performed using KAPA Library Preparation Kit (Kapa Biosystems, #KK8201) using Agilent's SureSelect Human All Exon V5 backbone with custom probes. The targeted DNA panel developed by Ashion (formerly known as the GEM Cancer panel) consisted of exonic probes against 541 cancer genes. Both panel and WXS assays contained 44,000 probes across evenly spaced genomic loci used for genome-wide copy number analysis. For the panel, additional probes tiled across intronic regions of 22 known tumor suppressor genes and 22 genes involved in common cancer translocations for structural analysis. All extractions and library preparations were performed according to manufacturer's instructions.

CBTN samples

Blood, tissue, and cell line DNA/RNA extractions were performed at the Biorepository Core at CHOP. Briefly, 10-20 mg frozen tissue, 0.4-1ml of blood or 2×10^6 cells pellet was used for extractions. Tissues were lysed using a Qiagen TissueLyser II (Qiagen) with 2×30 sec at 18Hz settings using 5 mm steel beads (cat# 69989, Qiagen). Both tissue and cell pellets processes included a CHCl₃ extraction and were run on the QIAcube automated platform (Qiagen) using the AllPrep DNA/RNA/miRNA Universal kit (cat# 80224, Qiagen). Blood was thawed and treated with RNase A (cat#, 19101, Qiagen); 0.4-1ml was processed using the Qiagen QIAsymphony automated platform (Qiagen) using the QIAsymphony DSP DNA Midi Kit (cat# 937255, Qiagen). DNA and RNA quantity and quality was assessed by PerkinElmer DropletQuant UV-VIS spectrophotometer (PerkinElmer) and an Agilent 4200 TapeStation (Agilent, USA) for RINe and DIne (RNA Integrity Number equivalent and DNA Integrity Number equivalent respectively). Library preparation and sequencing was performed by the NantHealth sequencing center. Briefly, DNA sequencing libraries were prepared for tumor and matched-normal DNA using the KAPA HyperPrep kit (cat# KK8541, Roche); tumor RNA-Seq libraries were prepared using KAPA Stranded RNA-Seq with RiboErase kit (cat# KK8484, Roche). Whole genome sequencing (WGS) was performed at an average depth of coverage of 60X for tumor samples and 30X for germline. The panel tumor sample was sequenced to 470X and the normal panel sample was sequenced to 308X. RNA samples were sequenced to an average of 200M reads. All samples were sequenced on the Illumina HiSeq platform (X/400) (Illumina) with 2 × 150bp read length.

Data generation

NantHealth Sequencing Center (Culver City, CA) performed whole genome sequencing (WGS) on all paired tumor (~60X) and constitutive (~30X) DNA samples. WGS libraries were 2x150 bp and sequenced on an Illumina X/400. NantHealth Sequencing Center performed ribosomal-depleted whole transcriptome stranded RNA-Seq to an average depth of 100M reads for CBTN tumor samples. The Translational Genomic Research Institute (TGEN; Phoenix, AZ) performed paired tumor (~200X) and constitutive whole exome sequencing (WXS) or targeted DNA panel (panel) and poly-A selected RNA-Seq (~200M reads) for PNOC tumor samples. PNOC WXS and RNA-Seq libraries 2x100 bp and sequenced on an Illumina HiSeq 2500.

DNA WGS Alignment

We used BWA-MEM [6] v0.7.17 for alignment of paired-end DNA-seq reads. We used version 38, patch release 12 of the *Homo sapiens* genome as our alignment reference, which we obtained as a FASTA file from UCSC [7]. Alignments were further processed using following the Broad Institute's Best Practices [8] for processing Binary Alignment/Map files (BAMs) in preparation for variant discovery.

Duplicates were marked using SAMBLASTER [9] v0.1.24, BAMs merged and sorted using Sambamba [10] v0.6.3. Resultant BAMs were processed using Broad's Genome Analysis Tool Kit (GATK) (<https://software.broadinstitute.org/gatk/>) v4.0.3.0, BaseRecalibrator submodule. Lastly, for normal/germline input, we run the GATK HaplotypeCaller [11] submodule on the recalibrated BAM, generating a genomic variant call format (GVCF) file. This file is used as the basis for germline calling, described in the "SNV calling for B-allele Frequency (BAF) generation" section. References can be obtained from the [Broad Genome References on AWS](#) bucket, with a general description of references here [12].

Quality Control of Sequencing Data

NGSCheckmate [13] was performed on matched tumor/normal CRAM files to confirm sample matches and remove mismatched samples from the dataset. CRAM inputs were preprocessed using BCFtools to filter and call 20k common single nucleotide polymorphisms (SNPs) using default parameters[14] and the resulting VCFs were used to run NGSCheckmate using [this workflow](#) in the D3b GitHub repository. Per author guidelines, <= 0.61 was used as a correlation coefficient cutoff at sequencing depths >10 to predict mismatched samples. For RNA-Seq, read strandedness was determined by running the [infer_experiment.py script](#) on the first 200k mapped reads. If calculated strandedness did not match strandedness information received from the sequencing center, samples were removed from analysis. We required at least 60% of RNA-Seq reads mapped to the human reference or samples were removed from analysis. MEND QC [15] was performed on aligned RNA-Seq reads using [this workflow](#) to identify mapped exonic non-duplicate reads.

Germline Variant Calling

SNP calling for B-allele Frequency (BAF) generation

Germline haplotype calls were performed following the [GATK Joint Genotyping Workflow](#), except the workflow was run on an individual sample basis. This workflow was applied to the GVCF output from the alignment workflow on normal/germline samples. Using only SNPs, we applied the [GATK generic hard filter suggestions](#) to the VCF, with an additional requirement of 10 reads minimum depth per SNP. This filtered VCF was used as input to Control-FREEC and CNVkit (below) for generation of BAF files. GATK v4.0.12.0 was used for all steps except VariantFiltration, which used 3.8.0 because as of GATK 4.0.12.0, this tool was beta and known to be unreliable for this purpose. This single-sample workflow can be found in the [Kids First GitHub repository](#). References can be obtained from the [Broad Genome References on AWS](#) bucket, with a general description of references here [12].

Somatic Mutation Calling

SNV and indel calling

For PBTA samples, we used four variant callers to call SNVs and indels from targeted DNA panel, WXS, and WGS data: Strelka2 [16], Mutect2 [17], Lancet [18], and VarDict [19]. WXS samples from TCGA were run using Strelka2, Mutect2 and Lancet. TCGA samples were captured using different WXS target capture kits and all the BED files were downloaded from [GDC portal](#). The input interval BED files for both panel and WXS data for PBTA samples were provided by the manufacturers. For both PBTA and TCGA, all panel and WXS BED files were padded by 100 bp on each side during Strelka2, Mutect2, and VarDict runs and 400 bp for the Lancet run.

For WGS calling, we utilized the non-padded BROAD Institute interval calling list [wgs_calling_regions.hg38.interval_list](#), comprised of the full genome minus N bases, unless otherwise noted below. Strelka2 [16] v2.9.3 was run using default parameters for canonical chromosomes (chr1-22, X,Y,M), as recommended by the authors. The final Strelka2 VCF was filtered

for PASS variants. Mutect2 from GATK v4.1.1.0 was run following Broad best practices outlined from their Workflow Description Language (WDL) [20]. The final Mutect2 VCF was filtered for PASS variants. To manage memory issues, VarDictJava [19] v1.58 [21] was run using 20Kb interval chunks of the input BED, padded by 100 bp on each side, such that if an indel occurred in between intervals, it would be captured. Parameters and filtering followed [BCBIO standards](#) except that variants with a variant allele frequency (VAF) ≥ 0.05 (instead of ≥ 0.10) were retained. The 0.05 VAF increased the true positive rate for indels and decreased the false positive rate for SNVs when using VarDict in consensus calling. The final VCF was filtered for PASS variants with TYPE=StronglySomatic. Lancet v1.0.7 was run using default parameters, except for those noted below. For input intervals to Lancet WGS, a reference BED was created by using only the UTR, exome, and start/stop codon features of the GENCODE 31 reference, augmented as recommended with PASS variant calls from Strelka2 and Mutect2 [22]. These intervals were then padded by 300 bp on each side during Lancet variant calling. Per recommendations by the New York Genome Center [22], for WGS samples, the Lancet input intervals described above were augmented with PASS variant calls from Strelka2 and Mutect2 as validation.

VCF annotation and MAF creation

Normalization of INDELs using `bcftools norm` [23] was performed on all PASS VCFs using the following subworkflow [24], release v3. The ENSEMBL Variant Effect Predictor [25], reference release 93, was used to annotate variants and bcftools was used to add population allele frequency (AF) from gnomAD. SNV and INDEL hotspots from v2 of MSKCC's database [26] plus the C228T and C250T TERT promoter mutations [27] were annotated. SNVs were annotated by matching amino acid position (`Protein_position` column in MAF file) with SNVs in the MSKCC database, splice sites were matched to `HGVSp_Short` values in the MSKCC database, and INDELs were matched based on amino acid present within the range of INDEL hotspots values in the MSKCC database. Non-hotspot annotated variants with a normal depth of ≤ 7 and/or gnomAD AF > 0.001 were removed as potential germline variants. TERT promoter mutations were matched using hg38 coordinates from [27]: C228T occurs at 5:1295113, is annotated as existing variant `s1242535815`, `COSM1716563`, `COSM1716558`, and is 66bp away from TSS and C250T occurs at Chr5:1295135, is annotated as existing variant `COSM1716559`, and is 88 bp away from TSS.

The final set of variants were retained if annotated as PASS or HotSpotAllele=1. MAFs were created using MSKCC's `vcf2maf` [28] v1.6.17.

Gather SNV and INDEL Hotspots

All variant calls from Strelka2, Mutect2, or Lancet that overlap with an SNV or INDEL hotspot from v2 of MSKCC's database [26] or the C228T and C250T TERT promoter mutations [27] were retained in a hotspot-specific MAF file, which was used for select analyses as described in the methods below. VarDict-only calls were not retained since ~ 39M calls with low VAF were uniquely called and may be potential false positives.

Consensus SNV Calling

Our SNV calling process led to separate sets of predicted mutations for each caller. We considered mutations to describe the same change if they were identical for the following MAF fields: `Chromosome`, `Start_Position`, `Reference_Allele`, `Allele`, and `Tumor_Sample_Barcode`. Strelka2 does not call multinucleotide variants (MNV), but instead calls each component SNV as a separate mutation, so we separated MNV calls from Mutect2 and Lancet into consecutive SNVs before comparing them with Strelka2. We examined the variant allele frequencies produced by each caller and compared their overlap with each other [29]. VarDict calls included many variants that were not

identified by other callers [30], while the other callers produced results that were relatively consistent with one another. Many of these VarDict-specific calls were variants with low allele frequency [31]. We termed mutations shared among the other three callers (Strelka2, Mutect2, and Lancet) to be consensus mutation calls and dropped VarDict due to concerns about it calling a large number of false positives. In practice, because our filtered set was based on the intersection of these three sets and because VarDict called nearly every mutation from the other three callers plus many that were unique to it, the decision to not consider VarDict calls has little impact on the results.

For some downstream analyses, only coding sequence SNVs (based on GENCODE v27 [32]) are used, to enhance comparability to other studies. We considered base pairs to be *effectively surveyed* if they were in the intersection of the genomic ranges considered by the callers used to generate the consensus and where appropriate, regions of interest, such as coding sequences. This definition of *effectively surveyed* base pairs is what is used to calculate effective genome size for calculations for tumor mutation burden and mutational signatures.

Recurrently mutated genes and co-occurrence of gene mutations

Using the consensus SNV calls, we identified genes that were recurrently mutated in the cohort, including nonsynonymous mutations with a variant allele frequency greater than 5% among the set of independent samples. The set of nonsynonymous mutations was determined using ENSEMBL Variant Effect Predictor [25] annotations, including High and Moderate consequence types as defined in `maf-tools` [33]. For each gene, we then tallied the number of samples that had at least one nonsynonymous mutation.

For genes that contained nonsynonymous mutations in multiple samples, we calculated pairwise mutation co-occurrence scores. This score was defined as the $I \times -\log_{10}(P)$ where I is 1 when the odds ratio is > 1 (indicating co-occurrence), and -1 when the odds ratio is < 1 (indicating mutual exclusivity), with P defined by Fisher's Exact Test.

Somatic Copy Number Variant Calling (WGS samples only)

We used Control-FREEC [34,35] v11.6 and CNVkit [36] v0.9.3 for copy number variant calls. For both algorithms, the `germline_sex_estimate` (described below) was used as input for sample sex and germline variant calls (above) were used as input for BAF estimation. Control-FREEC was run on human genome reference hg38 using the optional parameters of a 0.05 coefficient of variation, ploidy choice of 2-4, and BAF adjustment for tumor-normal pairs. Theta2 [37] used VarDict germline and somatic calls, filtered on PASS and strongly somatic, to infer tumor purity. Theta2 purity was added as an optional parameter to CNVkit to adjust copy number calls. CNVkit was run on human genome reference hg38 using the optional parameters of Theta2 purity and BAF adjustment for tumor-normal pairs. We used GISTIC [38] v.2.0.23 on the CNVkit and the consensus CNV segmentation files to generate gene-level copy number abundance (Log R Ratio) as well as chromosomal arm copy number alterations using the parameters specified in the [OpenPBTA Analysis repository](#).

Consensus CNV Calling

For each caller and sample, CNVs were called based on consensus among Control-FREEC [34,35], CNVkit [36], and Manta [39]. CNVs called significant by Control-FREEC (p -value < 0.01) and Manta calls that passed all filters [40] were included in consensus calling. Sample and caller combination files with more than 2500 CNVs called were removed from the set; we expect these to be noisy and poor quality samples based on cutoffs used in GISTIC [38]. For each sample, the following regions are included in the final consensus set: 1) regions with reciprocal overlap of at least 50% between two of the three callers; 2) smaller CNV regions that are at least 90% covered by another caller. Any copy number

alteration that was not called by two or more callers was not included in the consensus file. For the samples that are included in the consensus file, if a certain region has a neutral call, copy number of NA is defined for that region. CNV regions within 10,000 bp of each other with the same direction of gain or loss were merged into single region. We filtered out any CNVs that overlapped 50% or more with immunoglobulin, telomeric, centromeric, segment duplicated regions or were shorter than 3000 bp.

Focal Copy Number Calling

We added the ploidy inferred via Control-FREEC to the consensus CNV segmentation file and used the ploidy and copy number values to define gain and loss values broadly at the chromosome level. We used bedtools coverage [41,42] to add cytoband status using the UCSC cytoband file [43,44]. The output status call fractions, which are values of the loss, gain and callable fractions of each cytoband region, were used to define dominant status at the cytoband-level. The weighted means of each status call fraction were calculated using band length. We used the weighted means to define the dominant status at the chromosome arm-level.

A status is considered dominant if more than half of the region was callable and the status call fraction was greater than 0.9 for that region. The 0.9 threshold was chosen to ensure that the dominant status fraction call is greater than the remaining status fraction calls in a region.

We also wanted to define focal copy number units to avoid calling adjacent genes in the same cytoband or arm as copy number losses or gains where it would be more appropriate to call the broader region a loss or gain. For the determination of the most focal units, we first considered the dominant status calls at the chromosome arm-level. If the chromosome arm dominant status was not clearly defined as a gain or loss (and was callable) we looked to include the cytoband-level status call. Similarly, if a cytoband dominant status call was not clearly defined as a gain or loss (and was callable) we looked to include the gene-level status call. To obtain the gene-level data, we used the mergeByOverlaps function [45] from the IRanges package [46] to find overlaps between the segments in the consensus CNV file and the exons in the GENCODE v27 annotation file [32]. If the copy number value was 0, we set the status to “deep deletion”. For autosomes only, we set the status to “amplification” when the copy number value is greater than two times the ploidy value.

Somatic Structural Variant Calling (WGS samples only)

We used Manta SV [39] v1.4.0 for structural variant (SV) calls. Manta SV calling was also limited to regions used in Strelka2. The hg38 reference for SV calling used was limited to canonical chromosome regions. The somatic DNA workflow for SNV, indel, copy number, and SV calling can be found in the [KidsFirst Github repository](#). Manta SV output was annotated using [AnnotSV v2.1](#) [47] and the workflow can be found in the [D3b GitHub repository](#).

Gene Expression

Abundance Estimation

We used STAR [48] v2.6.1d to align paired-end RNA-seq reads. This output was used for all subsequent RNA analysis. We used Ensembl GENCODE 27 [32], “Comprehensive gene annotation” as a reference. We used RSEM [49] v1.3.1 for both FPKM and TPM transcript- and gene-level quantification. We also added a second method of quantification using kallisto [50] v0.43.1. This method differs in that it uses pseudoalignments using FASTQ reads directly to the aforementioned GENCODE 27 reference.

Gene Expression Matrices with Unique HUGO Symbols

Algorithms that perform gene set enrichment, molecular subtyping, or immune-profiling, for example, require an RNA-seq gene expression matrix as input, with HUGO gene symbols as row names and sample names as column names. There is a small proportion of gene symbols that map to multiple Ensembl gene identifiers (in GENCODE v27, 212 gene symbols map to 1866 Ensembl gene identifiers), termed multi-mapped gene symbols.

We first removed genes with no expression from the RSEM abundance data using a cut-off of FPKM > 0 in at least 1 sample across the PBTA cohort. We computed the mean FPKM across all samples per gene and for each multi-mapped gene symbol, we chose the Ensembl identifier corresponding to the maximum mean FPKM with the goal of choosing the identifier that best represented the expression of the gene. After collapsing gene identifiers, there were a total of 46,400 unique expressed genes in the poly-A dataset and a total of 53,011 unique expressed genes remaining in the stranded dataset. More detail can be found in the [collapse-rnaseq analysis module](#).

Immune Profiling/Deconvolution

We used the R package immunedecov [51,52] to deconvolute, quantify and compare various immune cell types across 21 histologies from the PBTA cohort with xCell [53] and CIBERSORT [54] in the stranded and poly-A collapsed FPKM RNA-seq datasets ([immune-deconv analysis module](#)). Both methods allow between samples (inter-sample), between cell types (intra-sample) and between cancer type (inter-histology) comparisons.

Gene Set Variation Analysis

We performed Gene Set Variation Analysis (GSVA) [55] on collapsed, log2-transformed RSEM FPKM data using the GSVA Bioconductor package [56] with setting `mx.diff=TRUE` to obtain Gaussian-distributed scores ([gene-set-enrichment-analysis analysis module](#)) for each of the MSigDB hallmark gene sets [57]. We compared GSVA scores among histology groups ([short_histology](#)) using ANOVA and subsequent Tukey tests; p-values were Bonferroni-corrected for multiple hypothesis testing.

Dimension reduction

We applied Uniform Manifold Approximation and Projection (UMAP) [58] to log2-transformed FPKM data using the `umap` R package [59]. We set the number of neighbors to 15 ([transcriptomic-dimension-reduction analysis module](#)).

RNA Fusion Calling and Prioritization

Gene fusion detection

We set up [Arriba v1.1.0](#) and STAR-Fusion 1.5.0 [60] fusion detection tools using CWL on CAVATICA. For both these tools we used aligned BAM and chimeric SAM files from STAR as inputs and GRCh38_gencode_v27 GTF for gene annotation. We ran STAR-Fusion with default parameters and annotated all fusion calls with GRCh38_v27_CTAT_lib_Feb092018.plug-n-play.tar.gz provided in the STAR-fusion release. For Arriba, we used a blacklist file (`blacklist_hg38_GRCh38_2018-11-04.tsv.gz`) from the Arriba release tarballs to remove recurrent fusion artifacts and transcripts present in healthy tissue. We also provided Arriba with strandedness information or set it to auto-detection for poly-A samples. We used [FusionAnnotator](#) on Arriba fusion calls in order to harmonize annotations with

those of STAR-Fusion. The RNA expression and fusion workflows can be found in the [KidsFirst GitHub repository](#) and the FusionAnnotator workflow found in the [D3b GitHub repository](#).

Fusion prioritization

We performed artifact filtering and additional annotation on fusion calls to prioritize putative oncogenic fusions. Briefly, we considered all in frame and frameshift fusion calls with a minimum of 1 junction reads and at least one gene partner expressed (TPM > 1) to be true calls. If a fusion call had large number of spanning fragment reads compared to junction reads (spanning fragment minus junction read greater than ten), we removed these calls as potential false positives. We prioritized a union of fusion calls as true calls if the fused genes were detected by both callers, the same fusion was recurrent within a `broad_histology` (>2 samples) or the fusion was specific to the `broad_histology`. If either 5' or 3' genes fused to more than five different genes within a sample, we removed these calls as potential false positives. We annotated putative driver fusions and prioritized fusions based on partners containing known [kinases](#), [oncogenes](#), [tumor suppressors](#), curated transcription factors [61], [COSMIC genes](#), and/or known [TCGA fusions](#) from curated [references](#). *MYBL1* [62], *SNCAIP* [63], *FOXR2* [64], *TTYH1* [65], and *TERT* [66,67,68,69] were added to the oncogene list and *BCOR* [64] and *QKI* [70] were added to the tumor suppressor gene list based on pediatric cancer literature review. The fusion filtering workflow can be found in the [OpenPBTA Analysis repository](#).

Mutational Signatures

We obtained weights for signature sets by applying deconstructSigs [71,72] to consensus SNVs with the BSgenome.Hsapiens.UCSC.hg38 annotations [73]. We estimated how many mutations contributed to each signature for each sample using each sample's signature weights. Weights for signatures fall in the range zero to one inclusive. For a given sample and signature combination, we estimated the number of contributing mutations per Mb of the genome by multiplying the signature weight by the total number of trinucleotide mutations identified by deconstructSigs and then dividing by the size of the effectively surveyed genome.

$$\frac{\# \text{ of contributing mutations}}{\text{Mb}} = \frac{\text{weight} * \sum \# \text{ Trinucleotide mutations}}{\text{Size in Mb of effectively surveyed genome}}$$

These results do not include signatures with small contributions; deconstructSigs drops signature weights that are less than 6% [71]. We used these methods to calculate signature scores for each sample with both COSMIC [74] and Alexandrov et al, 2013 [75] signature sets.

PBTA Tumor Mutation Burden

We consider tumor mutation burden (TMB) to be the number of consensus SNVs per *effectively surveyed* base of the genome.

$$\text{TMB} = \frac{\backslash\# \text{ of coding sequence SNVs}}{\text{Size in Mb of }\{\backslash\text{em effectively surveyed}\} \text{ genome}}$$

We used the total number coding sequence consensus SNVs for the numerator and the size of the intersection of the regions considered by Lancet, Strelka2, and Mutect2 with coding regions (CDS from GENCODE v27 annotation [32]) as the denominator.

TCGA Tumor Mutation Burden

We calculated tumor mutation burden in TCGA using MC3 mutation calls [76] for TCGA brain-related tumor projects including: LGG (lower-grade glioma) [77], GBM (glioblastoma multiforme) [78], and PCPG (pheochromocytoma and paraganglioma) [79]. The MC3 project provided an exome BED file. All SNVs fell within these regions. We considered the regions covered by the MC3 BED file (based on GENCODE v19 annotation [80]) to have been effectively surveyed.

Clinical Data Harmonization

WHO Classification of Disease Types

For the CBTN cohort, the `pathology_diagnosis` field in the `pbta-histologies.tsv` file contains a harmonized diagnosis based on the patient's pathology report. For the PNOC003 cohort, the `pathology_diagnosis` field in the `pbta-histologies.tsv` file contains the diagnosis gathered from the patient's pathology report. For the CBTN cohort, the `pathology_free_text_diagnosis` field in the `pbta-histologies.tsv` file contains additional free text diagnosis information gathered from the patient's pathology report. The `integrated_diagnosis` field in the `pbta-histologies.tsv` file is the standardized 2016 WHO diagnosis [81] based on `pathology_diagnosis`, molecular subtyping, and in some cases, additional pathology review. The `broad_histology` denotes the broad 2016 WHO classification for each tumor. The `short_histology` is an abbreviated version of either the `broad_histology` or `integrated_diagnosis` for plotting purposes. The `CNS_region` was subtyped into hemispheric, midline, mixed, or other based on specimen location (see table below).

Clinical and Histology Meta data	Definition	Possible values
<code>age_at_diagnosis_days</code>	Patient age at diagnosis in days	numeric
<code>age_last_update_days</code>	Patient age at the last clinical event/update in days	numeric
<code>aliquot_id</code>	External aliquot identifier	variable
<code>broad_composition</code>	Broad classification of sample type	cell-line;cyst;non-tumor;tumor
<code>broad_histology</code>	Broad WHO 2016 classification of cancer type	text
<code>cancer_predispositions</code>	Reported cancer predisposition syndromes	text
<code>cohort</code>	Scientific cohort	CBTN;PNOC

Clinical and Histology Meta data	Definition	Possible values
cohort_participant_id	Scientific cohort participant ID	C#####-C#####
composition	Sample composition	Derived Cell Line;Not Reported;Peripheral Whole Blood;Saliva;Solid Tissue
ethnicity	Patient reported ethnicity	text
experimental_strategy	Sequencing strategy	WGS;WXS;RNA-Seq;Panel
germline_sex_estimate	Predicted sex of patient based on germline X and Y ratio calculation (described in methods)	Female;Male;Unknown
CNS_region	Brain region based on primary_site	
integrated_diagnosis	2016 WHO diagnosis integrated from pathology diagnosis and molecular subtyping	text
Kids_First_Biospecimen_ID	KidsFirst biospecimen identifier	BS_#####
Kids_First_Participant_ID	KidsFirst patient identifier	PT_#####
molecular_subtype	Molecular subtype defined by WHO 2016 guidelines	text
normal_fraction	Theta2 normal DNA fraction estimate	numeric
Notes	Free text field describing changes from pathology_diagnosis to integrated_diagnosis or manner in which molecular_subtype was determined	text
OS_days	Overall survival in days	numeric

Clinical and Histology Metadata	Definition	Possible values
OS_status	Overall survival status	DECEASED;LIVING
parent_aliquot_id	External identifier combining sample_id, sample_type, aliquot_id, and sequencing_strategy for some samples	text
pathology_diagnosis	Reported and/or harmonized patient diagnosis from pathology reports	text
pathology_free_text_diagnosis	Free text patient diagnosis from pathology reports	text
primary_site	Bodily site(s) from which specimen was derived	text
race	Patient reported race	text
reported_gender	Patient reported gender	text
RNA_library	Type of RNA-Sequencing library preparation	stranded;poly-A
sample_id	External biospecimen identifier	variable
sample_type	Broad sample type	Normal;Tumor
seq_center	Sequencing center	BGI@CHOP Genome Center;Genomic Clinical Core at Sidra Medical and Research Center;NantOmics;TGEN
short_histology	Abbreviated integrated_diagnosis or broad_histology for plotting purposes	text
tumor_descriptor	Phase of therapy from which tumor was derived	Initial CNS Tumor;Progressive Disease Post-Mortem;Recurrence;Second Malignancy;Unavailable
tumor_fraction	Theta2 tumor DNA fraction estimate	numeric
tumor_ploidy	Control-FREEC ploidy	numeric

Table S1. Clinical metadata collected for OpenPBTA. {#tbl:S1}

CNS_region	primary_site
Hemispheric	Frontal Lobe,Temporal Lobe,Parietal Lobe,Occipital Lobe
Midline	Pons/Brainstem,Brain Stem- Midbrain/Tectum,Brain Stem- Pons,Brain Stem-Medulla,Thalamus,Basal Ganglia,Hippocampus,Pineal Gland
Spine	Spinal Cord- Cervical,Spinal Cord- Thoracic,Spinal Cord- Lumbar/Thecal Sac,Spine NOS
Ventricles	Ventricles
Posterior fossa	Cerebellum/Posterior Fossa
Optic pathway	Optic Pathway
Suprasellar	Suprasellar/Hypothalamic/Pituitary
Other	Meninges/Dura,Other locations NOS,Skull,Cranial Nerves NOS,Brain

Table S2. Harmonized CNS brain regions derived from primary site values. {#tbl:S2}

Molecular Subtyping

The `molecular_subtype` column in the `pbta-histologies.tsv` file contains molecular subtypes for tumor types selected from `pathology_diagnosis` and `pathology_free_text_diagnosis` fields as described below, following World Health Organization 2016 classification criteria [81].

Medulloblastoma (MB) subtypes SHH, MYC, Group 3, and Group 4 were predicted using the consensus of two RNA expression classifiers: [Medulloblastoma Classifier]](https://github.com/d3b-center/medullo-classifier-package) and MM2S Classifier [82] on the RSEM FPKM data.

High-grade glioma (HGG) subtypes were derived using the criteria below (additional details in the [analysis README](#)):

1. If any sample contained an H3F3A K28M, HIST1H3B K28M, HIST1H3C K28M, or HIST2H3C K28M mutation and no BRAF V600E mutation, it was subtyped as DMG, H3K28.
2. If any sample contained an HIST1H3B K28M, HIST1H3C K28M, or HIST2H3C K28M mutation and a BRAF V600E mutation, it was subtyped as DMG, H3 K28, BRAF V600E.
3. If any sample contained an H3F3A G35V or G35R mutation, it was subtyped as HGG, H3 G35.
4. If any high-grade glioma sample contained an IDH1 R132 mutation, it was subtyped as HGG, IDH.
5. If a sample was initially classified as HGAT, had no defining histone mutations, and a BRAF V600E mutation, it was subtyped as BRAF V600E.
6. All other high-grade glioma samples that did not meet any of these criteria were subtyped as HGG, H3 wildtype.

Non-MB and non-ATRT embryonal (Embryonal tumor in the `broad_histology` column of the metadata pbta-histologies.tsv) subtypes were derived using the criteria below [83,84,85,86]. Additional details can be found in the analysis [notebook](#).

1. Any RNA-seq biospecimen with *LIN28A* overexpression, plus a *TTYH1* fusion (5' partner) with a gene adjacent or within the C19MC miRNA cluster and/or copy number amplification of the C19MC

- region was subtyped as **ETMR**, **C19MC-altered** (Embryonal tumor with multilayer rosettes, chromosome 19 miRNA cluster altered).
2. Any RNA-seq biospecimen with *LIN28A* overexpression, a *TTYH1* fusion (5' partner) with a gene adjacent or within the C19MC miRNA cluster but no evidence of copy number amplification of the C19MC region was subtyped as **ETMR**, **NOS** (Embryonal tumor with multilayer rosettes, not otherwise specified).
 3. Any RNA-seq biospecimen with a fusion having a 5' *MN1* and 3' *BEND2* or *CXXC5* partner were subtyped as **CNS HGNET-MN1** (Central nervous system (CNS) high-grade neuroepithelial tumor with *MN1* alteration).
 4. Non-MB and non-ATRT embryonal tumors with internal tandem duplication of *BCOR* were subtyped as **CNS HGNET-BCOR** (CNS high-grade neuroepithelial tumor with *BCOR* alteration).
 5. Non-MB and non-ATRT embryonal tumors with over-expression and/or gene fusions in *FOXR2* were subtyped as **CNS NB-FOXR2** (CNS neuroblastoma with *FOXR2* activation).
 6. Non-MB and non-ATRT embryonal tumors with *CIC-NUTM1* or other *CIC* fusions, were subtyped as **CNS EFT-CIC** (CNS Ewing sarcoma family tumor with *CIC* alteration).
 7. Non-MB and non-ATRT embryonal tumors that did not fit any of the above categories were subtyped as CNS Embryonal, NOS (CNS Embryonal tumor, not otherwise specified).

TP53 Alteration Annotation

In addition to tumor types mentioned above, TP53 altered status is also annotated for all samples and if a sample is determined to be either **TP53 loss** or **TP53 activated**, this annotation will be included in the **molecular_subtype** column. We applied a *TP53* inactivation classifier originally trained on TCGA PanCan data [87] to the matched RNA expression data for each sample. Along with the *TP53* classifier scores, consensus SNV and CNV, SV, and references databases that list *TP53* hotspot mutations [26,88,89] and functional domains [90] were used collectively to determine *TP53* alteration status for each sample. The rules for calling either **TP53 loss** or **TP53 activated** are as follows: If a sample has any of the two well-characterized *TP53* gain-of-function mutations, p.R273C or p.R248W [91], **TP53 activated** status will be assigned. A sample will be annotated as **TP53 loss** if any of the following conditions is met: 1) It contains a *TP53* hotspot mutation as defined by IARC *TP53* database [26,88,89] 2) It contains two *TP53* alterations, including SNV, CNV or SV, which is indicative of probable bi-allelic alterations 3) It contains one *TP53* somatic alteration, including SNV, CNV, or SV and a germline *TP53* mutation indicated by the diagnosis of Li-Fraumeni syndrome [92] 4) It contains one germline *TP53* mutation indicated by Li-Fraumeni syndrome and the *TP53* classifier score for matched RNA-Seq is over 0.5.

Survival

Overall survival, denoted **OS_days**, was calculated as days since initial diagnosis.

Prediction of participants' genetic sex

The clinical metadata provided included a reported gender. We used DNA data, in concert with the reported gender, to predict participant genetic sex so that we could identify sexually dimorphic outcomes. This analysis could also reveal samples that may have been contaminated in certain circumstances. We used the idxstats utility from SAMtools [93] to calculate read lengths, the number of mapped reads, and the corresponding chromosomal location for reads to the X and Y chromosomes. We used the fraction of total normalized X and Y chromosome reads that were attributed to the Y chromosome as a summary statistic. We reviewed this statistic in the context of reported gender and determined that a threshold of less than 0.2 clearly delineated female samples. Fractions greater than 0.4 were predicted to be males. Samples with values in the range [0.2, 0.4]

were marked as unknown. We ran this analysis through [CWL](#) on Cavatica. Resulting calls were added to the clinical metadata as `germline_sex_estimate`.

Selection of independent samples

Certain analyses required that we select only a single representative specimen for each individual. In these cases, we prioritized primary tumors and those with whole-genome sequencing available. If this filtering still resulted in multiple specimens, we selected from the remaining set randomly.

Quantify Telomerase Activity using Gene Expression Data

We predicted telomerase activity of pediatric brain tumor samples using our recently developed method EXTEND. In brief, EXTEND estimates telomerase activity based on the expression of a 13-gene signature. This signature was derived by comparing telomerase positive tumors and tumors with activated alternative lengthening of telomeres pathway, a group presumably negative of telomerase activity. More details about the algorithm can be found in reference [94]. We calculated telomerase activity score for each sample of the PBTA cohort and examined the score distribution across both broad and specific disease histological subtypes. We also compared EXTEND scores across the four molecular subgroups of medulloblastoma (Group3, Group4, SHH and WNT) using a series of pairwise two-sample t-tests with a Bonferroni correction for multiple testing. EXTEND scores have been further compared, using Spearman rank correlation, between counts and FPKM gene expression values from poly-A and stranded protocols.

Results

Results section stub.

The Open Pediatric Brain Tumor Atlas

This section will introduce the dataset (e.g., the histologies represented and what data types are included; Figure 1A-B) and the process for contributing analytical code and to the manuscript (Figure 1C-D).

A

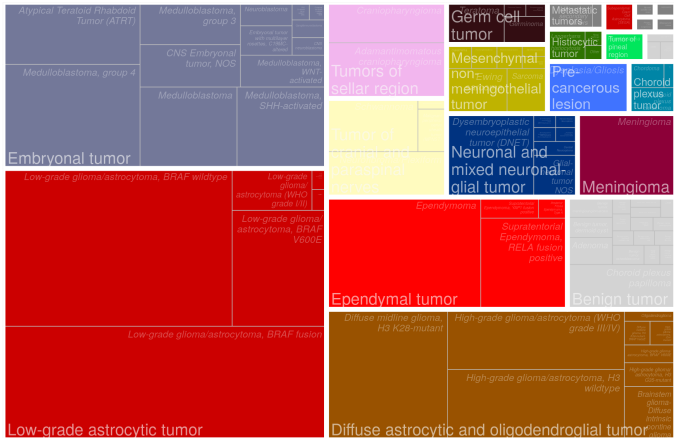


Figure 1: An overview of the OpenPBTA project. A) The distribution of unique participant samples across short histologies and integrated diagnoses.

Landscape of Genomic Alterations

The OncoPrint will provide a visualization of the genomic alterations found in the analyses implemented throughout the OpenPBTA project.

Figure 2: OncoPrint displaying genes most frequently altered across the OpenPBTA dataset. Genes include the top 50 most frequently mutated genes and the top 20 genes with copy number alterations. Samples were filtered to primary samples or, when no primary sample from an individual participant was available, a randomly selected sample with whole genome sequencing (WGS) data. Sample histology (`short_histology`) is displayed in the annotation bar at the bottom of the plot.

Landscape of Mutational Processes

This section summarizes the mutational landscape of the pediatric brain tumor samples of this dataset. Figure 1A shows the tumor mutation burden as compared to adult TCGA brain-related tumors. Figure 3B-C show concordance of these samples with mutational signatures from COSMIC [74] and Alexandrov et al, 2013 [75] signature sets.

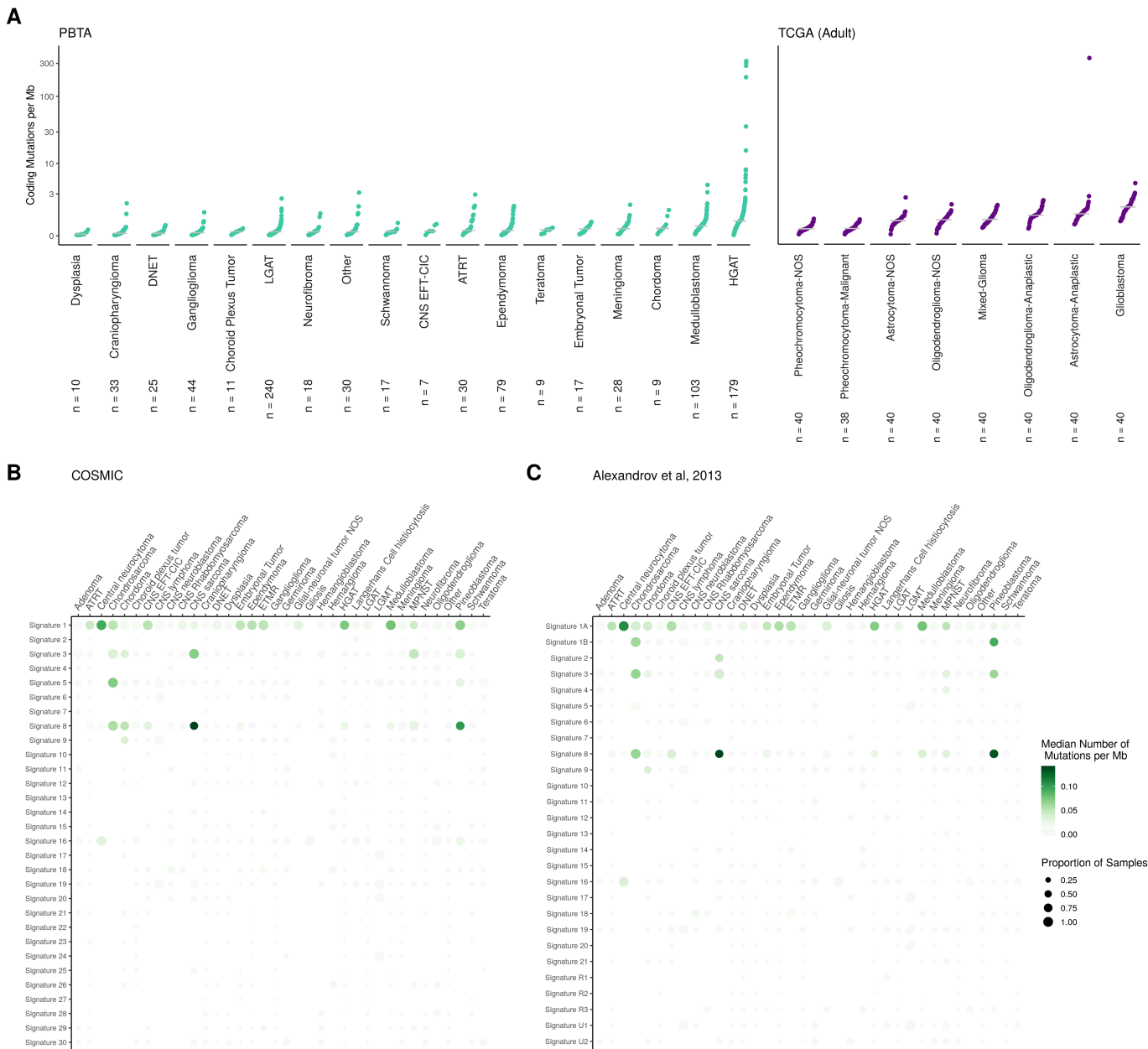


Figure 3: Mutational Landscape

Copy Number Variant Overview

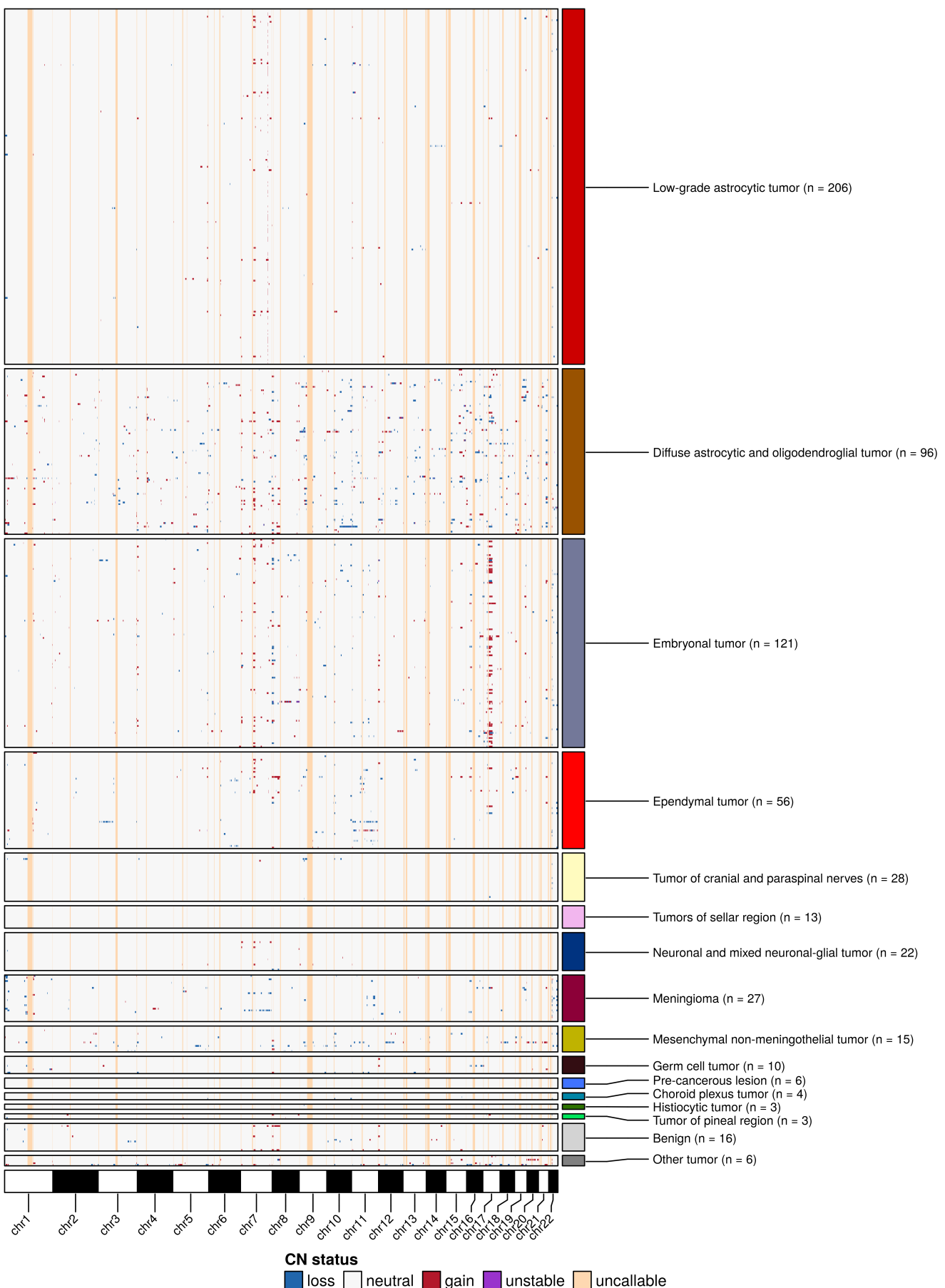


Figure 4: This figure shows dominant statuses for small copy number consensus segments (< 10 Mb) across the genome, where each square represents a ~1 Mb binned section of the genome. A dominant status is declared if one status is >75% coverage. Unstable indicates multiple non-neutral statuses totaling coverage >75%. Copy number segments longer than 10 Mb have been removed from the figure for easier interpretability.

Recurrence and co-occurrence of mutations

This section will discuss the genes and regions that are repeatedly mutated within and between cancer types. The occurrence of mutations in affecting particular genes, separated by tumor type is shown in Figure 5A, with significant co-occurrence across all types illustrated in Figure 5B.

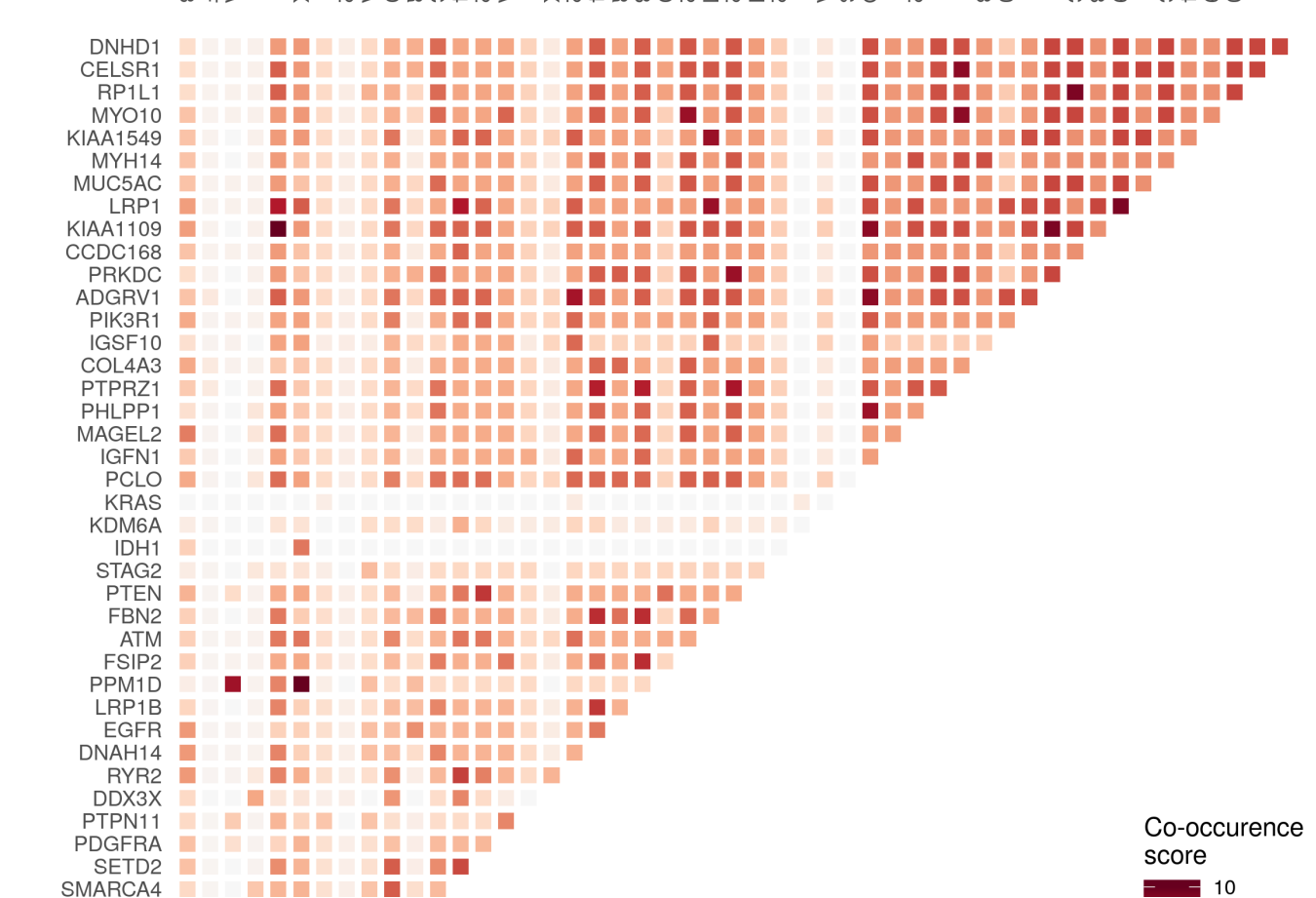
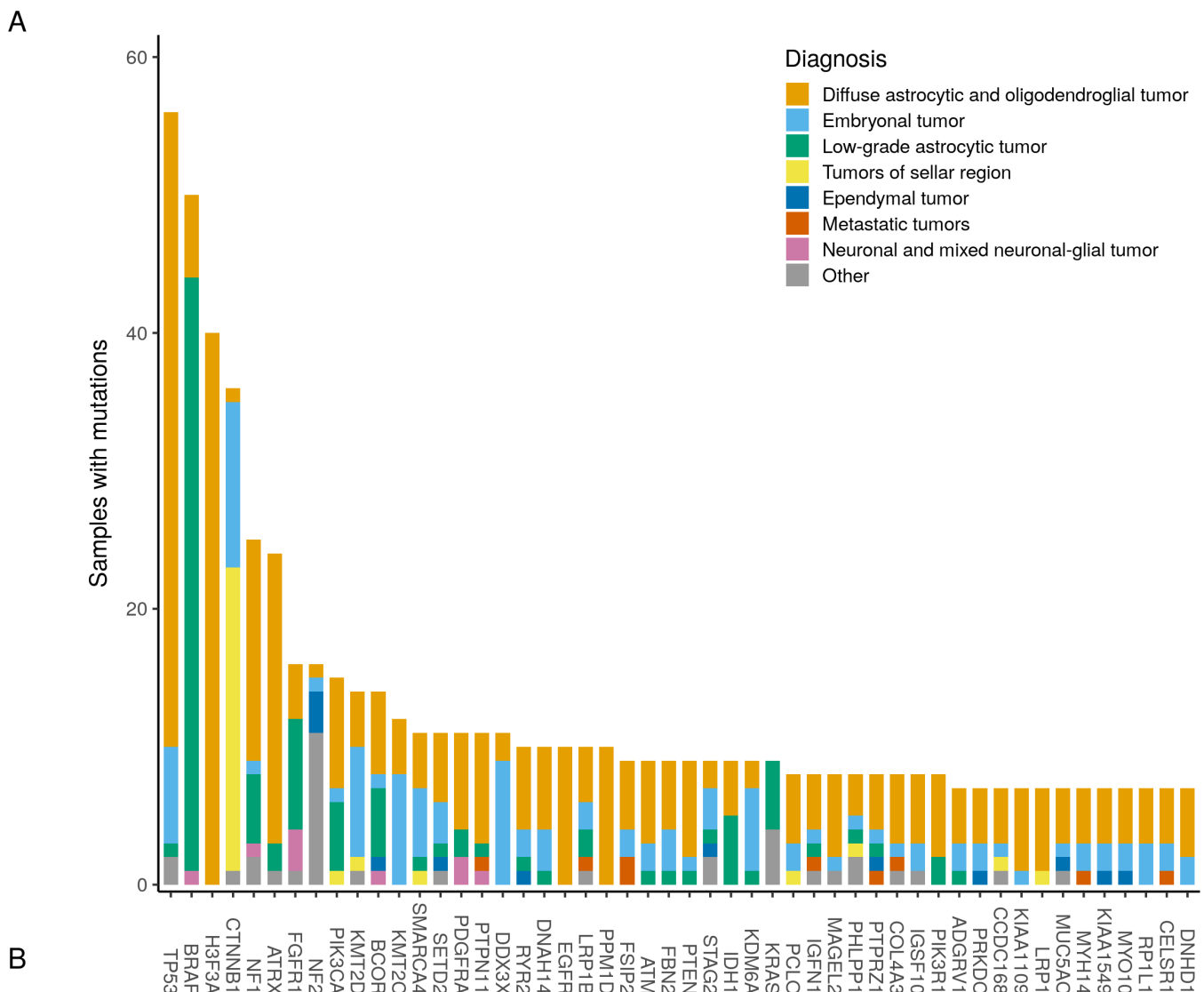




Figure 5: Occurrence and co-occurrence of nonsynonymous mutations for the 50 most commonly mutated genes across all tumor types. A) Counts of nonsynonymous mutations, colored by tumor type (as defined in `integrated_diagnosis`). B) Co-occurrence and mutual exclusivity of nonsynonymous mutations between genes. The co-occurrence score is defined as $I(-\log_{10}(P))$ where P is defined by Fisher's exact test and I is 1 when mutations co-occur more often than expected and -1 when exclusivity is more common.

Transcriptomic landscape

This section will discuss the overall structure of the transcriptome data, pathway analysis, and immune deconvolution. A dimension reduction plot, a heatmap of GSVA scores [55], and a heatmap of xCell fraction values [53] are shown in Figure 6.

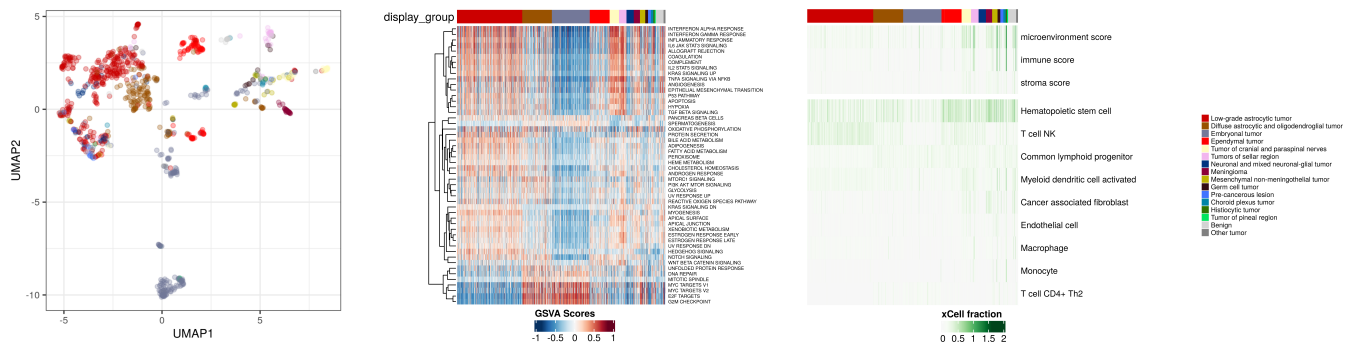


Figure 6: Transcriptomic overview (stranded data only) A) First two dimensions from Uniform Manifold Approximation and Projection (UMAP) of sample transcriptome data. Points are colored by `short_histology` of the samples they represent. B) Heatmap of GSVA scores for Hallmark gene sets with significant differences, with samples ordered by `short_histology`. C) Heatmap of xCell fraction values for scores and cell types with high variance, with samples ordered by `short_histology`.

Quantify Telomerase Activity using Gene Expression Data

We used gene expression data sets from both poly-A and stranded RNA-Seq protocols to predict telomerase activities using EXTEND [95] as shown in [Supplementary Tables](#).

For both platforms, EXTEND scores were highly consistent between FPKM versus counts data (Supplementary Figure) ZA and Figure ZB.

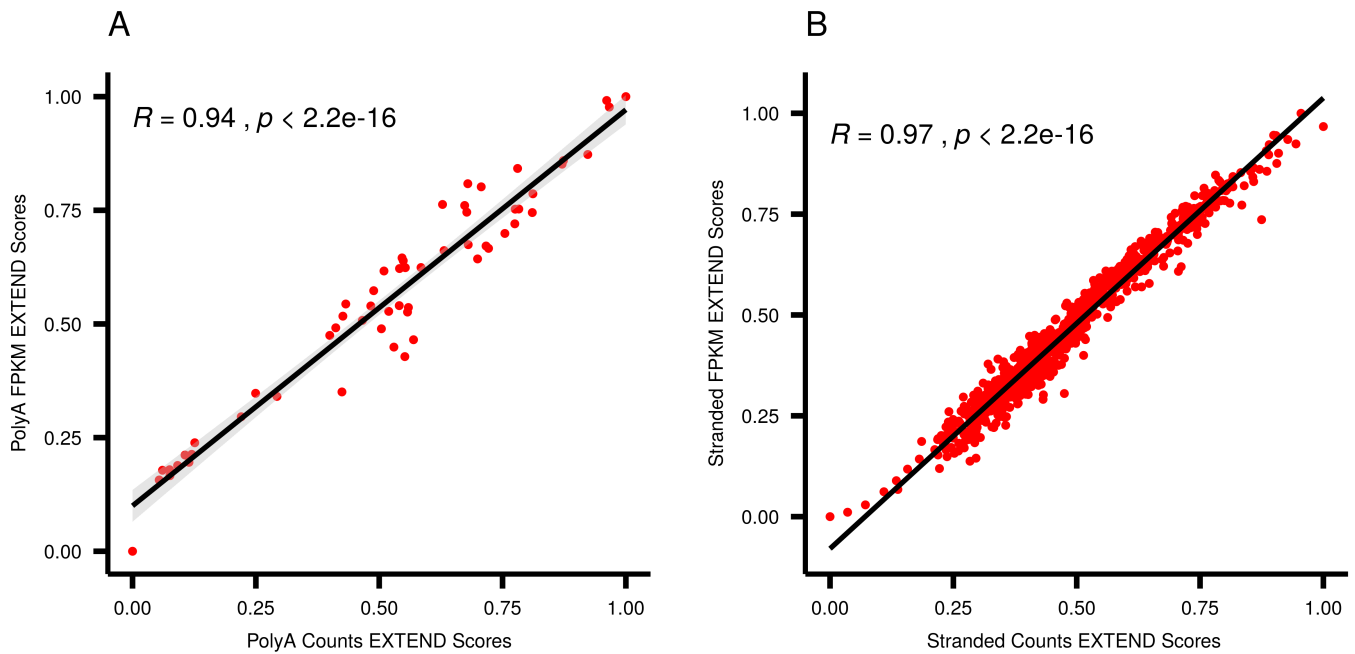


Figure 7: Scatter plots comparing telomerase activities via Spearman correlation for counts with FPKM format. A) poly-A platform . B) stranded platform .

We next examined telomerase activity across different brain tumor histological subtypes using data from the stranded FPKM protocol. Across the short histological groups, we found germinomas had the highest EXTEND scores. However, teratomas, another type of germ cell tumor, had much lower scores (Figure) 8A. Teratomas were previously reported to have negligible or low telomerase activities [96]. Teratomas originating from the tissue of three dermal layers of an embryo, are benign germ cell neoplasms [??? 10.1097/MOP.0b013e32832b41ee]. These tumors are divided into mature and immature (malignant) groups, where pediatric tumors are mostly classified as mature ones [??? 10.1016/j.jpedsurg.2004.03.045]. Mature tumors are deficient of malignant potential thereby reducing the risk of malignancy [??? 10.1016/j.jpedsurg.2004.03.045], hence bearing low telomerase activities. Benign neoplasia including dysplasia and hemangioblastomas had the lowest scores. Among common pediatric brain tumors, medulloblastomas had higher scores than high grade astrocytic tumors, ependymomas and low-grade astrocytomas. Across broad groups, benign tumors and precancerous lesions were among those with the lowest scores, whereas pineal region and embryonal tumors have the highest scores (Figure) 8B. Considering medulloblastoma tumors, high risk Group3 and Group4 subtypes had higher scores than WNT and SHH subtype (Figure) 8C. A similar pattern has been speculated with respect to cell of origin by one of the earlier studies [97] which mainly focused TERT promoter mutations for medulloblastoma subtypes comparisons rather than telomerase activity.

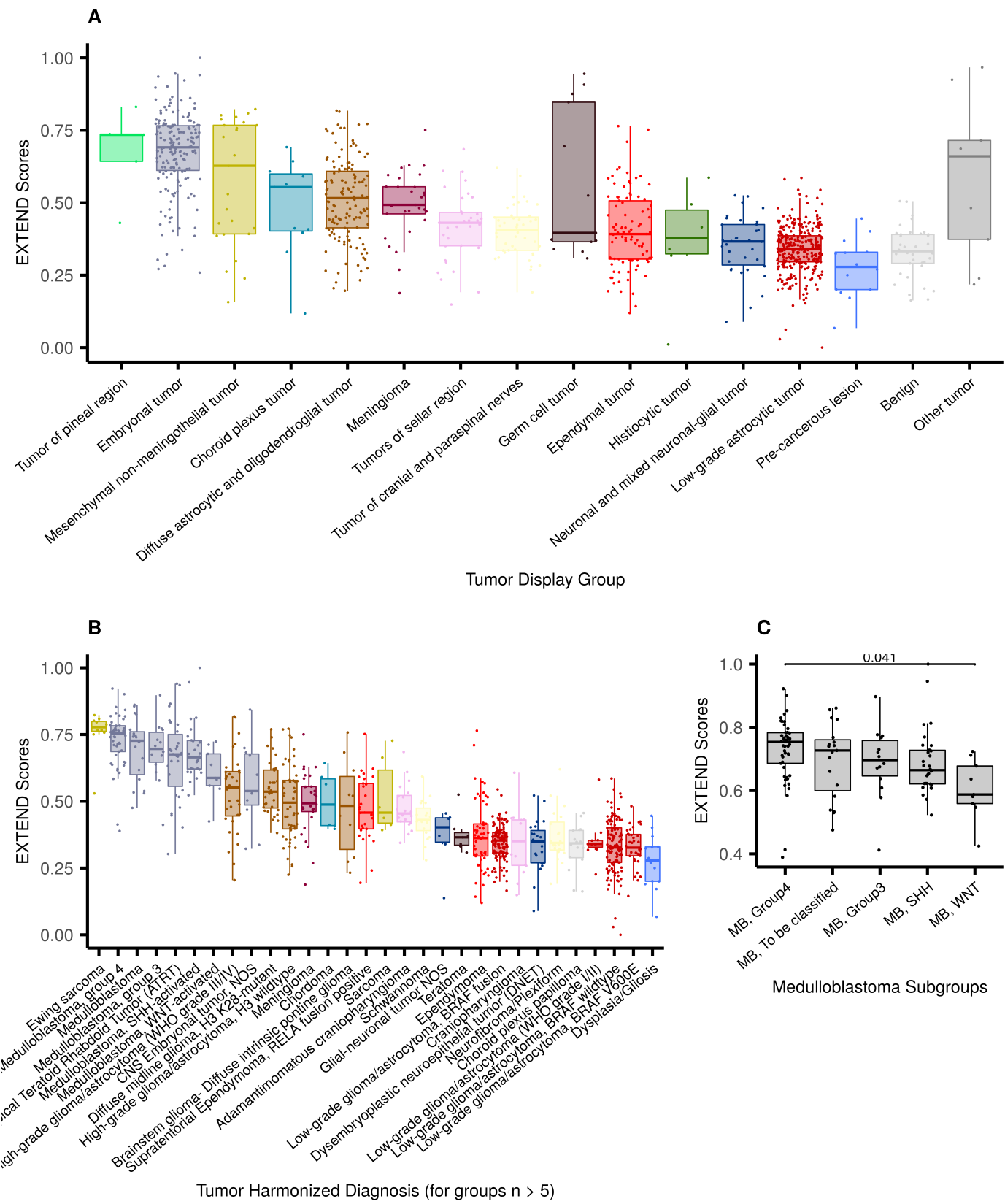


Figure 8: Box plots representing distribution of telomerase activities for stranded FPKM data. A) short histological classifications. B) broad histological classifications. C) Comparison of telomerase activities across molecular subtypes of medulloblastoma tumors. P-values have been calculated using series of two-sided t-tests and corrected via Bonferroni correction.

Conclusions

Stub in conclusions section

Data and Resource Availability

Author Contributions

Author	Contributions
Joshua A. Shapiro	Methodology, Software, Validation, Formal analysis, Investigation, Writing - Original draft, Writing - Review and editing, Visualization, Supervision
Candace L. Savonen	Methodology, Software, Validation, Formal analysis, Investigation, Writing - Original draft, Visualization
Chante J. Bethell	Methodology, Validation, Formal analysis, Investigation, Writing - Original draft, Visualization
Krutika S. Gaonkar	Data curation, Formal Analysis, Investigation, Methodology, Software, Writing – original draft
Yuankun Zhu	Data curation, Formal Analysis, Investigation, Methodology, Supervision
Miguel A. Brown	Data curation, Methodology
Nhat Duong	Formal Analysis, Investigation, Methodology
Komal S. Rathi	Formal Analysis, Investigation, Methodology, Writing – original draft
Nighat Noureen	Formal analysis, Visualization, Writing - Original draft
Bo Zhang	Data curation, Formal Analysis
Brian M. Ennis	Data curation, Formal Analysis
Stephanie J. Spielman	Validation, Formal analysis, Writing - Review and editing, Visualization, Supervision
Bailey Farrow	Data curation, Software
Nicolas Van Kuren	Data curation, Software
Tejaswi Koganti	Formal Analysis, Investigation
Shrivats Kannan	Formal Analysis, Methodology, Writing – original draft
Pichai Raman	Conceptualization, Formal Analysis, Methodology
Jennifer Mason	Supervision
Daniel P. Miller	Formal Analysis
Anna R. Poetsch	Formal Analysis
Payal Jain	Data curation, Investigation, Validation
Adam A. Kraya	Methodology
Allison P. Heath	Project administration
Mateusz P. Koptyra	Formal Analysis, Writing – original draft
Yiran Guo	Formal Analysis
Xiaoyan Huang	Formal Analysis
Jessica Wong	Writing – original draft
Mariarita Santi	Investigation, Validation

Author	Contributions
Angela Viaene	Investigation, Validation
Laura Scolaro	Data Curation
Angela Waanders	Supervision
Derek Hanson	Validation
Hongbo M. Xie	Methodology, Supervision
Siyuan Zheng	Formal analysis, Visualization, Writing - Original draft, Supervision
Cassie N. Kline	Supervision
Jena V. Lilly	Conceptualization, Funding acquisition, Project administration
Philip B. Storm	Conceptualization, Funding acquisition, Resources
Adam C. Resnick	Conceptualization, Funding acquisition, Resources, Supervision
Jo Lynne Rokita	Conceptualization, Data curation, Formal Analysis, Funding acquisition, Investigation, Methodology, Software, Supervision, Writing – original draft
Casey S. Greene	Conceptualization, Funding acquisition, Methodology, Project administration, Software, Supervision, Writing – review & editing
Jaclyn N. Taroni	Methodology, Software, Validation, Formal analysis, Investigation, Data curation, Writing - Review and editing, Visualization, Supervision, Project administration
Children's Brain Tumor Tissue Consortium	Conceptualization
Pacific Pediatric Neurooncology Consortium	Conceptualization

Acknowledgments

Conflicts of Interest

CSG's spouse is an employee of Alex's Lemonade Stand Foundation, which was a sponsor of this research.

References

1. Children's Brain Tumor Network <https://cbtn.org/>
2. Working Together to Put Kids First <https://kidsfirstdrc.org/>
3. Pediatric High Grade Glioma Resources From the Children's Brain Tumor Tissue Consortium (CBTTC) and Pediatric Brain Tumor Atlas (PBTA)
Heba Ijaz, Mateusz Koptyra, Krutika S. Gaonkar, Jo Lynne Rokita, Valerie P. Baubet, Lamiya Tauhid, Yankun Zhu, Miguel Brown, Gonzalo Lopez, Bo Zhang, ... Children's Brain Tumor Tissue Consortium
Cold Spring Harbor Laboratory (2019-05-31) <https://doi.org/gf6qt>
DOI: [10.1101/656587](https://doi.org/10.1101/656587)
4. Pacific Pediatric Neuro-Oncology Consortium <https://pnoc.us/>
5. A pilot precision medicine trial for children with diffuse intrinsic pontine glioma—PNOC003: A report from the Pacific Pediatric Neuro-Oncology Consortium
Sabine Mueller, Payal Jain, Winnie S. Liang, Lindsay Kilburn, Cassie Kline, Nalin Gupta, Eshini Panditharatna, Suresh N. Magge, Bo Zhang, Yuankun Zhu, ... Adam C. Resnick
International Journal of Cancer (2019-04-03) <https://doi.org/gf6pfb>
DOI: [10.1002/ijc.32258](https://doi.org/10.1002/ijc.32258) · PMID: [30861105](#)
6. Aligning sequence reads, clone sequences and assembly contigs with BWA-MEM
Heng Li
arXiv (2013-05-28) <https://arxiv.org/abs/1303.3997>
7. Index of /goldenPath/hg38/bigZips <http://hgdownload.soe.ucsc.edu/goldenPath/hg38/bigZips/>
8. <https://software.broadinstitute.org/gatk/best-practices/workflow?id>
9. SAMBLASTER: fast duplicate marking and structural variant read extraction
G. G. Faust, I. M. Hall
Bioinformatics (2014-05-07) <https://doi.org/f6kft3>
DOI: [10.1093/bioinformatics/btu314](https://doi.org/10.1093/bioinformatics/btu314) · PMID: [24812344](#) · PMCID: [PMC4147885](#)
10. Sambamba: fast processing of NGS alignment formats
Artem Tarasov, Albert J. Vilella, Edwin Cuppen, Isaac J. Nijman, Pjotr Prins
Bioinformatics (2015-06-15) <https://doi.org/gfzsfw>
DOI: [10.1093/bioinformatics/btv098](https://doi.org/10.1093/bioinformatics/btv098) · PMID: [25697820](#) · PMCID: [PMC4765878](#)
11. Scaling accurate genetic variant discovery to tens of thousands of samples
Ryan Poplin, Valentin Ruano-Rubio, Mark A. DePristo, Tim J. Fennell, Mauricio O. Carneiro, Geraldine A. Van der Auwera, David E. Kling, Laura D. Gauthier, Ami Levy-Moonshine, David Roazen, ... Eric Banks
Cold Spring Harbor Laboratory (2018-07-24) <https://doi.org/ggmrvr>
DOI: [10.1101/201178](https://doi.org/10.1101/201178)
12. Broad Genome References <https://s3.amazonaws.com/broad-references/broad-references-readme.html>

13. **NGSCheckMate: software for validating sample identity in next-generation sequencing studies within and across data types**
Sejoon Lee, Soohyun Lee, Scott Ouellette, Woong-Yang Park, Eunjung A. Lee, Peter J. Park
Nucleic Acids Research (2017-06-20) <https://doi.org/f9xrq4>
DOI: [10.1093/nar/gkx193](https://doi.org/10.1093/nar/gkx193) · PMID: [28369524](https://pubmed.ncbi.nlm.nih.gov/28369524/) · PMCID: [PMC5499645](https://pubmed.ncbi.nlm.nih.gov/PMC5499645/)
14. **GitHub - parklab/NGSCheckMate: Software program for checking sample matching for NGS data**
GitHub
<https://github.com/parklab/NGSCheckMate>
15. **The case for using Mapped Exonic Non-Duplicate (MEND) read counts in RNA-Seq experiments: examples from pediatric cancer datasets**
Holly C. Beale, Jacquelyn M. Roger, Matthew A. Cattle, Liam T. McKay, Drew K. A. Thomson, Katrina Learned, A. Geoffrey Lyle, Ellen T. Kephart, Rob Currie, Du Linh Lam, ... Olena M. Vaske
Cold Spring Harbor Laboratory (2020-08-26) <https://doi.org/gghzj8>
DOI: [10.1101/716829](https://doi.org/10.1101/716829)
16. **Strelka2: fast and accurate calling of germline and somatic variants**
Sangtae Kim, Konrad Scheffler, Aaron L. Halpern, Mitchell A. Bekritsky, Eunho Noh, Morten Källberg, Xiaoyu Chen, Yeonbin Kim, Doruk Beyer, Peter Krusche, Christopher T. Saunders
Nature Methods (2018-07-16) <https://doi.org/gdwrp4>
DOI: [10.1038/s41592-018-0051-x](https://doi.org/10.1038/s41592-018-0051-x) · PMID: [30013048](https://pubmed.ncbi.nlm.nih.gov/30013048/)
17. **Calling Somatic SNVs and Indels with Mutect2**
David Benjamin, Takuto Sato, Kristian Cibulskis, Gad Getz, Chip Stewart, Lee Lichtenstein
Cold Spring Harbor Laboratory (2019-12-02) <https://doi.org/ggnttw>
DOI: [10.1101/861054](https://doi.org/10.1101/861054)
18. **Genome-wide somatic variant calling using localized colored de Bruijn graphs**
Giuseppe Narzisi, André Corvelo, Kanika Arora, Ewa A. Bergmann, Minita Shah, Rajeeva Musunuri, Anne-Katrin Emde, Nicolas Robine, Vladimir Vacic, Michael C. Zody
Communications Biology (2018-03-22) <https://doi.org/gfcfr8>
DOI: [10.1038/s42003-018-0023-9](https://doi.org/10.1038/s42003-018-0023-9) · PMID: [30271907](https://pubmed.ncbi.nlm.nih.gov/30271907/) · PMCID: [PMC6123722](https://pubmed.ncbi.nlm.nih.gov/PMC6123722/)
19. **VarDict: a novel and versatile variant caller for next-generation sequencing in cancer research**
Zhongwu Lai, Aleksandra Markovets, Miika Ahdesmaki, Brad Chapman, Oliver Hofmann, Robert McEwen, Justin Johnson, Brian Dougherty, J. Carl Barrett, Jonathan R. Dry
Nucleic Acids Research (2016-06-20) <https://doi.org/f8v6qz>
DOI: [10.1093/nar/gkw227](https://doi.org/10.1093/nar/gkw227) · PMID: [27060149](https://pubmed.ncbi.nlm.nih.gov/27060149/) · PMCID: [PMC4914105](https://pubmed.ncbi.nlm.nih.gov/PMC4914105/)
20. **gatk/mutect2.wdl at 4.1.1.0 · broadinstitute/gatk**
GitHub
<https://github.com/broadinstitute/gatk>
21. **GitHub - AstraZeneca-NGS/VarDictJava: VarDict Java port**
GitHub
<https://github.com/AstraZeneca-NGS/VarDictJava>
22. **Deep sequencing of 3 cancer cell lines on 2 sequencing platforms**
Kanika Arora, Minita Shah, Molly Johnson, Rashesh Sanghvi, Jennifer Shelton, Kshithija Nagulapalli, Dayna M. Oschwald, Michael C. Zody, Soren Germer, Vaidehi Jobanputra, ... Nicolas Robine

23. **bcftools(1)** <http://samtools.github.io/bcftools/bcftools.html#norm>
24. **OpenPBTA-workflows/kfdrc_annot_vcf_sub_wf.cwl** at master · d3b-center/OpenPBTA-workflows
GitHub
<https://github.com/d3b-center/OpenPBTA-workflows>
25. **The Ensembl Variant Effect Predictor**
William McLaren, Laurent Gil, Sarah E. Hunt, Harpreet Singh Riat, Graham R. S. Ritchie, Anja Thormann, Paul Flicek, Fiona Cunningham
Genome Biology (2016-06-06) <https://doi.org/gdz75c>
DOI: [10.1186/s13059-016-0974-4](https://doi.org/10.1186/s13059-016-0974-4) · PMID: [27268795](https://pubmed.ncbi.nlm.nih.gov/27268795/) · PMCID: [PMC4893825](https://pubmed.ncbi.nlm.nih.gov/PMC4893825/)
26. **Cancer Hotspots** <https://www.cancerhotspots.org/>
27. **Activating Telomerase TERT Promoter Mutations and Their Application for the Detection of Bladder Cancer**
Maria Zvereva, Eduard Pisarev, Ismail Hosen, Olga Kisil, Simon Matskeplishvili, Elena Kubareva, David Kamalov, Alexander Tivtikyan, Arnaud Manel, Emmanuel Vian, ... Florence Le Calvez-Kelm
International Journal of Molecular Sciences (2020-08-21) <https://doi.org/gmf45b>
DOI: [10.3390/jjms21176034](https://doi.org/10.3390/jjms21176034) · PMID: [32839402](https://pubmed.ncbi.nlm.nih.gov/32839402/) · PMCID: [PMC7503716](https://pubmed.ncbi.nlm.nih.gov/PMC7503716/)
28. **GitHub - mskcc/vcf2maf: Convert a VCF into a MAF, where each variant is annotated to only one of all possible gene isoforms**
GitHub
<https://github.com/mskcc/vcf2maf>
29. **OpenPBTA-analysis/compare_snv_callers_plots.Rmd** at master · AlexsLemonade/OpenPBTA-analysis
GitHub
<https://github.com/AlexsLemonade/OpenPBTA-analysis>
30. https://github.com/AlexsLemonade/OpenPBTA-analysis/blob/master/analyses/snvcallers/plots/comparison/upset_plot.png
31. https://github.com/AlexsLemonade/OpenPBTA-analysis/blob/master/analyses/snvcallers/plots/comparison/vaf_violin_plot.png
32. **GENCODE - Human Release 27** https://www.gencodegenes.org/human/release_27.html
33. **Maftools: efficient and comprehensive analysis of somatic variants in cancer**
Anand Mayakonda, De-Chen Lin, Yassen Assenov, Christoph Plass, H. Phillip Koeffler
Genome Research (2018-11) <https://doi.org/gfmnwf>
DOI: [10.1101/gr.239244.118](https://doi.org/10.1101/gr.239244.118) · PMID: [30341162](https://pubmed.ncbi.nlm.nih.gov/30341162/) · PMCID: [PMC6211645](https://pubmed.ncbi.nlm.nih.gov/PMC6211645/)
34. **Control-FREEC: a tool for assessing copy number and allelic content using next-generation sequencing data**
Valentina Boeva, Tatiana Popova, Kevin Bleakley, Pierre Chiche, Julie Cappo, Gudrun Schleiermacher, Isabelle Janoueix-Lerosey, Olivier Delattre, Emmanuel Barillot

35. Control-free calling of copy number alterations in deep-sequencing data using GC-content normalization

Valentina Boeva, Andrei Zinovyev, Kevin Bleakley, Jean-Philippe Vert, Isabelle Janoueix-Lerosey, Olivier Delattre, Emmanuel Barillot

Bioinformatics (2011-01-15) <https://doi.org/c6bcps>

DOI: [10.1093/bioinformatics/btq635](https://doi.org/10.1093/bioinformatics/btq635) · PMID: [21081509](#) · PMCID: [PMC3018818](#)

36. CNVkit: Genome-Wide Copy Number Detection and Visualization from Targeted DNA Sequencing

Eric Talevich, A. Hunter Shain, Thomas Botton, Boris C. Bastian

PLOS Computational Biology (2016-04-21) <https://doi.org/c9pd>

DOI: [10.1371/journal.pcbi.1004873](https://doi.org/10.1371/journal.pcbi.1004873) · PMID: [27100738](#) · PMCID: [PMC4839673](#)

37. Quantifying tumor heterogeneity in whole-genome and whole-exome sequencing data

Layla Oesper, Gryte Satas, Benjamin J. Raphael

Bioinformatics (2014-12-15) <https://doi.org/f6rmgt>

DOI: [10.1093/bioinformatics/btu651](https://doi.org/10.1093/bioinformatics/btu651) · PMID: [25297070](#) · PMCID: [PMC4253833](#)

38. GISTIC2.0 facilitates sensitive and confident localization of the targets of focal somatic copy-number alteration in human cancers

Craig H Mermel, Steven E Schumacher, Barbara Hill, Matthew L Meyerson, Rameen Beroukhim, Gad Getz

Genome Biology (2011-04-28) <https://doi.org/dzhjqh>

DOI: [10.1186/gb-2011-12-4-r41](https://doi.org/10.1186/gb-2011-12-4-r41) · PMID: [21527027](#) · PMCID: [PMC3218867](#)

39. Manta: rapid detection of structural variants and indels for germline and cancer sequencing applications

Xiaoyu Chen, Ole Schulz-Trieglaff, Richard Shaw, Bret Barnes, Felix Schlesinger, Morten Källberg, Anthony J. Cox, Semyon Kruglyak, Christopher T. Saunders

Bioinformatics (2016-04-15) <https://doi.org/gf3ggb>

DOI: [10.1093/bioinformatics/btv710](https://doi.org/10.1093/bioinformatics/btv710) · PMID: [26647377](#)

40. manta/README.md at 75b5c38d4fcdf6961197b28a41eb61856f2d976 · Illumina/manta

GitHub

<https://github.com/Illumina/manta>

41. coverage — bedtools 2.30.0 documentation

<https://bedtools.readthedocs.io/en/latest/content/tools/coverage.html>

42. BEDTools: a flexible suite of utilities for comparing genomic features

Aaron R. Quinlan, Ira M. Hall

Bioinformatics (2010-03-15) <https://doi.org/cmrrms3>

DOI: [10.1093/bioinformatics/btq033](https://doi.org/10.1093/bioinformatics/btq033) · PMID: [20110278](#) · PMCID: [PMC2832824](#)

43. <http://hgdownload.cse.ucsc.edu/goldenpath/hg38/database/cytoBand.txt.gz>

44. The UCSC Genome Browser database: extensions and updates 2013

Laurence R. Meyer, Ann S. Zweig, Angie S. Hinrichs, Donna Karolchik, Robert M. Kuhn, Matthew Wong, Cricket A. Sloan, Kate R. Rosenbloom, Greg Roe, Brooke Rhead, ... W. James Kent

45. findOverlaps-methods function - RDocumentation

<https://www.rdocumentation.org/packages/IRanges/versions/2.6.1/topics/findOverlaps-methods>

46. Software for Computing and Annotating Genomic Ranges

Michael Lawrence, Wolfgang Huber, Hervé Pagès, Patrick Aboyou, Marc Carlson, Robert Gentleman, Martin T. Morgan, Vincent J. Carey

PLoS Computational Biology (2013-08-08) <https://doi.org/f5cmfg>

DOI: [10.1371/journal.pcbi.1003118](https://doi.org/10.1371/journal.pcbi.1003118) · PMID: [23950696](https://pubmed.ncbi.nlm.nih.gov/23950696/) · PMCID: [PMC3738458](https://pubmed.ncbi.nlm.nih.gov/PMC3738458/)

47. AnnotSV: an integrated tool for structural variations annotation

Véronique Geoffroy, Yvan Herenger, Arnaud Kress, Corinne Stoetzel, Amélie Piton, Hélène Dollfus, Jean Muller

Bioinformatics (2018-10-15) <https://doi.org/gdcs3>

DOI: [10.1093/bioinformatics/bty304](https://doi.org/10.1093/bioinformatics/bty304) · PMID: [29669011](https://pubmed.ncbi.nlm.nih.gov/29669011/)

48. STAR: ultrafast universal RNA-seq aligner

Alexander Dobin, Carrie A. Davis, Felix Schlesinger, Jorg Drenkow, Chris Zaleski, Sonali Jha, Philippe Batut, Mark Chaisson, Thomas R. Gingeras

Bioinformatics (2013-01) <https://doi.org/f4h523>

DOI: [10.1093/bioinformatics/bts635](https://doi.org/10.1093/bioinformatics/bts635) · PMID: [23104886](https://pubmed.ncbi.nlm.nih.gov/23104886/) · PMCID: [PMC3530905](https://pubmed.ncbi.nlm.nih.gov/PMC3530905/)

49. RSEM: accurate transcript quantification from RNA-Seq data with or without a reference genome

Bo Li, Colin N Dewey

BMC Bioinformatics (2011-08-04) <https://doi.org/cwg8n5>

DOI: [10.1186/1471-2105-12-323](https://doi.org/10.1186/1471-2105-12-323) · PMID: [21816040](https://pubmed.ncbi.nlm.nih.gov/21816040/) · PMCID: [PMC3163565](https://pubmed.ncbi.nlm.nih.gov/PMC3163565/)

50. Near-optimal probabilistic RNA-seq quantification

Nicolas L Bray, Harold Pimentel, Pál Melsted, Lior Pachter

Nature Biotechnology (2016-04-04) <https://doi.org/f8nvsp>

DOI: [10.1038/nbt.3519](https://doi.org/10.1038/nbt.3519) · PMID: [27043002](https://pubmed.ncbi.nlm.nih.gov/27043002/)

51. Comprehensive evaluation of transcriptome-based cell-type quantification methods for immuno-oncology.

Gregor Sturm, Francesca Finotello, Florent Petitprez, Jitao David Zhang, Jan Baumbach, Wolf H Fridman, Markus List, Tatsiana Aneichyk

Bioinformatics (Oxford, England) (2019-07-15) <https://www.ncbi.nlm.nih.gov/pubmed/31510660>

DOI: [10.1093/bioinformatics/btz363](https://doi.org/10.1093/bioinformatics/btz363) · PMID: [31510660](https://pubmed.ncbi.nlm.nih.gov/31510660/) · PMCID: [PMC6612828](https://pubmed.ncbi.nlm.nih.gov/PMC6612828/)

52. GitHub - icbi-lab/immunedeconv: A unified interface to immune deconvolution methods (CIBERSORT, EPIC, quanTIseq, TIMER, xCell, MCPcounter)

GitHub

<https://github.com/icbi-lab/immunedeconv>

53. xCell: digitally portraying the tissue cellular heterogeneity landscape

Dvir Aran, Zicheng Hu, Atul J. Butte

Genome Biology (2017-11-15) <https://doi.org/gckmj5>

DOI: [10.1186/s13059-017-1349-1](https://doi.org/10.1186/s13059-017-1349-1) · PMID: [29141660](https://pubmed.ncbi.nlm.nih.gov/29141660/) · PMCID: [PMC5688663](https://pubmed.ncbi.nlm.nih.gov/PMC5688663/)

54. Robust enumeration of cell subsets from tissue expression profiles

Aaron M Newman, Chih Long Liu, Michael R Green, Andrew J Gentles, Weiguo Feng, Yue Xu, Chuong D Hoang, Maximilian Diehn, Ash A Alizadeh
Nature Methods (2015-03-30) <https://doi.org/gcp3f5>
DOI: [10.1038/nmeth.3337](https://doi.org/10.1038/nmeth.3337) · PMID: [25822800](https://pubmed.ncbi.nlm.nih.gov/25822800/) · PMCID: [PMC4739640](https://pubmed.ncbi.nlm.nih.gov/PMC4739640/)

55. GSVA: gene set variation analysis for microarray and RNA-Seq data

Sonja Hänelmann, Robert Castelo, Justin Guinney
BMC Bioinformatics (2013) <https://doi.org/gb8vx5>
DOI: [10.1186/1471-2105-14-7](https://doi.org/10.1186/1471-2105-14-7) · PMID: [23323831](https://pubmed.ncbi.nlm.nih.gov/23323831/) · PMCID: [PMC3618321](https://pubmed.ncbi.nlm.nih.gov/PMC3618321/)

56. GSVA

Justin Guinney [Aut, Cre], Robert Castelo [Aut], Joan Fernandez[Ctb]
Bioconductor (2017) <https://doi.org/ggxrgs>
DOI: [10.18129/b9.bioc.gsava](https://doi.org/10.18129/b9.bioc.gsava)

57. The Molecular Signatures Database Hallmark Gene Set Collection

Arthur Liberzon, Chet Birger, Helga Thorvaldsdóttir, Mahmoud Ghandi, Jill P. Mesirov, Pablo Tamayo
Cell Systems (2015-12) <https://doi.org/gf78hq>
DOI: [10.1016/j.cels.2015.12.004](https://doi.org/10.1016/j.cels.2015.12.004) · PMID: [26771021](https://pubmed.ncbi.nlm.nih.gov/26771021/) · PMCID: [PMC4707969](https://pubmed.ncbi.nlm.nih.gov/PMC4707969/)

58. UMAP: Uniform Manifold Approximation and Projection for Dimension Reduction

Leland McInnes, John Healy, James Melville
arXiv (2018-02-09) <https://arxiv.org/abs/1802.03426v2>

59. <https://cran.r-project.org/package>

60. STAR-Fusion: Fast and Accurate Fusion Transcript Detection from RNA-Seq

Brian J. Haas, Alex Dobin, Nicolas Stransky, Bo Li, Xiao Yang, Timothy Tickle, Asma Bankapur, Carrie Ganote, Thomas G. Doak, Nathalie Pochet, ... Aviv Regev
Cold Spring Harbor Laboratory (2017-03-24) <https://doi.org/gf5pc5>
DOI: [10.1101/120295](https://doi.org/10.1101/120295)

61. The Human Transcription Factors

Samuel A. Lambert, Arttu Jolma, Laura F. Campitelli, Pratyush K. Das, Yimeng Yin, Mihai Albu, Xiaoting Chen, Jussi Taipale, Timothy R. Hughes, Matthew T. Weirauch
Cell (2018-02) <https://doi.org/gcw8rb>
DOI: [10.1016/j.cell.2018.01.029](https://doi.org/10.1016/j.cell.2018.01.029) · PMID: [29425488](https://pubmed.ncbi.nlm.nih.gov/29425488/)

62. Genomic analysis of diffuse pediatric low-grade gliomas identifies recurrent oncogenic truncating rearrangements in the transcription factor MYBL1

L. A. Ramkissoon, P. M. Horowitz, J. M. Craig, S. H. Ramkissoon, B. E. Rich, S. E. Schumacher, A. McKenna, M. S. Lawrence, G. Bergthold, P. K. Brastianos, ... K. L. Ligon
Proceedings of the National Academy of Sciences (2013-04-30) <https://doi.org/f42gg4>
DOI: [10.1073/pnas.1300252110](https://doi.org/10.1073/pnas.1300252110) · PMID: [23633565](https://pubmed.ncbi.nlm.nih.gov/23633565/) · PMCID: [PMC3657784](https://pubmed.ncbi.nlm.nih.gov/PMC3657784/)

63. Subgroup-specific structural variation across 1,000 medulloblastoma genomes

Paul A. Northcott, David J. H. Shih, John Peacock, Livia Garzia, A. Sorana Morrissy, Thomas Zichner, Adrian M. Stütz, Andrey Korshunov, Jüri Reimand, Steven E. Schumacher, ... Michael D. Taylor
Nature (2012-07-25) <https://doi.org/ggdhk3>
DOI: [10.1038/nature11327](https://doi.org/10.1038/nature11327) · PMID: [22832581](https://pubmed.ncbi.nlm.nih.gov/22832581/) · PMCID: [PMC3683624](https://pubmed.ncbi.nlm.nih.gov/PMC3683624/)

64. New Brain Tumor Entities Emerge from Molecular Classification of CNS-PNETs

Dominik Sturm, Brent A. Orr, Umut H. Toprak, Volker Hovestadt, David T.W. Jones, David Capper, Martin Sill, Ivo Buchhalter, Paul A. Northcott, Irina Leis, ... Marcel Kool
Cell (2016-02) <https://doi.org/f3t869>
DOI: [10.1016/j.cell.2016.01.015](https://doi.org/10.1016/j.cell.2016.01.015) · PMID: [26919435](https://pubmed.ncbi.nlm.nih.gov/26919435/) · PMCID: [PMC5139621](https://pubmed.ncbi.nlm.nih.gov/PMC5139621/)

65. Fusion of TTYH1 with the C19MC microRNA cluster drives expression of a brain-specific DNMT3B isoform in the embryonal brain tumor ETMR

Claudia L Kleinman, Noha Gerges, Simon Papillon-Cavanagh, Patrick Sin-Chan, Albena Pramatarova, Dong-Anh Khuong Quang, Véronique Adoue, Stephan Busche, Maxime Caron, Haig Djambazian, ... Nada Jabado
Nature Genetics (2013-12-08) <https://doi.org/ggdhk4>
DOI: [10.1038/ng.2849](https://doi.org/10.1038/ng.2849) · PMID: [24316981](https://pubmed.ncbi.nlm.nih.gov/24316981/)

66. TERT rearrangements are frequent in neuroblastoma and identify aggressive tumors

Linda J Valentijn, Jan Koster, Danny A Zwijnenburg, Nancy E Hasselt, Peter van Sluis, Richard Volckmann, Max M van Noesel, Rani E George, Godelieve AM Tytgat, Jan J Molenaar, Rogier Versteeg
Nature Genetics (2015-11-02) <https://doi.org/ggdhk5>
DOI: [10.1038/ng.3438](https://doi.org/10.1038/ng.3438) · PMID: [26523776](https://pubmed.ncbi.nlm.nih.gov/26523776/)

67. Recurrent pre-existing and acquired DNA copy number alterations, including focal TERT gains, in neuroblastoma central nervous system metastases

David Cobrinik, Irina Ostrovnaya, Maryam Hassimi, Satish K. Tickoo, Irene Y. Cheung, Nai-Kong V. Cheung
Genes, Chromosomes and Cancer (2013-12) <https://doi.org/f5gd94>
DOI: [10.1002/gcc.22110](https://doi.org/10.1002/gcc.22110) · PMID: [24123354](https://pubmed.ncbi.nlm.nih.gov/24123354/)

68. Activation of human telomerase reverse transcriptase through gene fusion in clear cell sarcoma of the kidney

Jenny Karlsson, Henrik Lilljebjörn, Linda Holmquist Mengelbier, Anders Valind, Marianne Rissler, Ingrid Øra, Thoas Fioretos, David Gisselsson
Cancer Letters (2015-02) <https://doi.org/f25ck5>
DOI: [10.1016/j.canlet.2014.11.057](https://doi.org/10.1016/j.canlet.2014.11.057) · PMID: [25481751](https://pubmed.ncbi.nlm.nih.gov/25481751/)

69. New Molecular Considerations for Glioma: IDH, ATRX, BRAF, TERT, H3 K27M

Michael Karsy, Jian Guan, Adam L. Cohen, Randy L. Jensen, Howard Colman
Current Neurology and Neuroscience Reports (2017-03-07) <https://doi.org/ggdhk2>
DOI: [10.1007/s11910-017-0722-5](https://doi.org/10.1007/s11910-017-0722-5) · PMID: [28271343](https://pubmed.ncbi.nlm.nih.gov/28271343/)

70. MYB-QKI rearrangements in angiocentric glioma drive tumorigenicity through a tripartite mechanism

Pratiti Bandopadhyay, Lori A Ramkissoon, Payal Jain, Guillaume Bergthold, Jeremiah Wala, Rhamy Zeid, Steven E Schumacher, Laura Urbanski, Ryan O'Rourke, William J Gibson, ... Adam C Resnick
Nature Genetics (2016-02-01) <https://doi.org/f8bwqn>
DOI: [10.1038/ng.3500](https://doi.org/10.1038/ng.3500) · PMID: [26829751](https://pubmed.ncbi.nlm.nih.gov/26829751/) · PMCID: [PMC4767685](https://pubmed.ncbi.nlm.nih.gov/PMC4767685/)

71. deconstructSigs: delineating mutational processes in single tumors distinguishes DNA repair deficiencies and patterns of carcinoma evolution

Rachel Rosenthal, Nicholas McGranahan, Javier Herrero, Barry S. Taylor, Charles Swanton
Genome Biology (2016-02-22) <https://doi.org/f8bdsq>
DOI: [10.1186/s13059-016-0893-4](https://doi.org/10.1186/s13059-016-0893-4) · PMID: [26899170](https://pubmed.ncbi.nlm.nih.gov/26899170/) · PMCID: [PMC4762164](https://pubmed.ncbi.nlm.nih.gov/PMC4762164/)

72. GitHub - raeroose01/deconstructSigs: deconstructSigs

GitHub

<https://github.com/raeroose01/deconstructSigs>

73. BSgenome.Hsapiens.UCSC.hg38

Bioconductor

<http://bioconductor.org/packages/BSgenome.Hsapiens.UCSC.hg38/>

74. COSMIC - Catalogue of Somatic Mutations in Cancer

Cosmic

<https://cancer.sanger.ac.uk/cosmic>

75. Signatures of mutational processes in human cancer

Ludmil B. Alexandrov, Serena Nik-Zainal, David C. Wedge, Samuel A. J. R. Aparicio, Sam Behjati, Andrew V. Biankin, Graham R. Bignell, Niccolò Bolli, Ake Borg, Anne-Lise Børresen-Dale, ... ICGC PedBrain

Nature (2013-08-14) <https://doi.org/f22m2q>

DOI: [10.1038/nature12477](https://doi.org/10.1038/nature12477) · PMID: [23945592](https://pubmed.ncbi.nlm.nih.gov/23945592/) · PMCID: [PMC3776390](https://pmcid.ncbi.nlm.nih.gov/pmc/articles/PMC3776390/)

76. Scalable Open Science Approach for Mutation Calling of Tumor Exomes Using Multiple Genomic Pipelines

Kyle Ellrott, Matthew H. Bailey, Gordon Saksena, Kyle R. Covington, Cyriac Kandoth, Chip Stewart, Julian Hess, Singer Ma, Kami E. Chiotti, Michael McLellan, ... Armaz Mariamidze

Cell Systems (2018-03) <https://doi.org/gf9twn>

DOI: [10.1016/j.cels.2018.03.002](https://doi.org/10.1016/j.cels.2018.03.002) · PMID: [29596782](https://pubmed.ncbi.nlm.nih.gov/29596782/) · PMCID: [PMC6075717](https://pmcid.ncbi.nlm.nih.gov/pmc/articles/PMC6075717/)

77. Comprehensive, Integrative Genomic Analysis of Diffuse Lower-Grade Gliomas

The Cancer Genome Atlas Research Network

New England Journal of Medicine (2015-06-25) <https://doi.org/f7f82c>

DOI: [10.1056/nejmoa1402121](https://doi.org/10.1056/nejmoa1402121) · PMID: [26061751](https://pubmed.ncbi.nlm.nih.gov/26061751/) · PMCID: [PMC4530011](https://pmcid.ncbi.nlm.nih.gov/pmc/articles/PMC4530011/)

78. The Somatic Genomic Landscape of Glioblastoma

Cameron W. Brennan, Roel G.W. Verhaak, Aaron McKenna, Benito Campos, Houtan Noushmehr, Sofie R. Salama, Siyuan Zheng, Debyani Chakravarty, J. Zachary Sanborn, Samuel H. Berman, ... Roger McLendon

Cell (2013-10) <https://doi.org/f5dbzj>

DOI: [10.1016/j.cell.2013.09.034](https://doi.org/10.1016/j.cell.2013.09.034) · PMID: [24120142](https://pubmed.ncbi.nlm.nih.gov/24120142/) · PMCID: [PMC3910500](https://pmcid.ncbi.nlm.nih.gov/pmc/articles/PMC3910500/)

79. Comprehensive Molecular Characterization of Pheochromocytoma and Paraganglioma

Lauren Fishbein, Ignaty Leshchiner, Vonn Walter, Ludmila Danilova, A. Gordon Robertson, Amy R. Johnson, Tara M. Lichtenberg, Bradley A. Murray, Hans K. Ghayee, Tobias Else, ... Erik Zmuda

Cancer Cell (2017-02) <https://doi.org/f9vcmf>

DOI: [10.1016/j.ccr.2017.01.001](https://doi.org/10.1016/j.ccr.2017.01.001) · PMID: [28162975](https://pubmed.ncbi.nlm.nih.gov/28162975/) · PMCID: [PMC5643159](https://pmcid.ncbi.nlm.nih.gov/pmc/articles/PMC5643159/)

80. GENCODE - Human Release 19 https://www.gencodegenes.org/human/release_19.html

81. The 2016 World Health Organization Classification of Tumors of the Central Nervous System: a summary

David N. Louis, Arie Perry, Guido Reifenberger, Andreas von Deimling, Dominique Figarella-Branger, Webster K. Cavenee, Hiroko Ohgaki, Otmar D. Wiestler, Paul Kleihues, David W. Ellison

Acta Neuropathologica (2016-05-09) <https://doi.org/f8mspx>

DOI: [10.1007/s00401-016-1545-1](https://doi.org/10.1007/s00401-016-1545-1) · PMID: [27157931](https://pubmed.ncbi.nlm.nih.gov/27157931/)

82. MM2S: personalized diagnosis of medulloblastoma patients and model systems

Deena M. A. Gendoo, Benjamin Haibe-Kains

Source Code for Biology and Medicine (2016-04-11) <https://doi.org/ghcqf2>

DOI: [10.1186/s13029-016-0053-y](https://doi.org/10.1186/s13029-016-0053-y) · PMID: [27069505](https://pubmed.ncbi.nlm.nih.gov/27069505/) · PMCID: [PMC4827218](https://pubmed.ncbi.nlm.nih.gov/PMC4827218/)

83. Embryonal Tumors of the Central Nervous System in Children: The Era of Targeted Therapeutics.

David E Kram, Jacob J Henderson, Muhammad Baig, Diya Chakraborty, Morgan A Gardner, Subhasree Biswas, Soumen Khatua

Bioengineering (Basel, Switzerland) (2018-09-23) <https://www.ncbi.nlm.nih.gov/pubmed/30249036>

DOI: [10.3390/bioengineering5040078](https://doi.org/10.3390/bioengineering5040078) · PMID: [30249036](https://pubmed.ncbi.nlm.nih.gov/30249036/) · PMCID: [PMC6315657](https://pubmed.ncbi.nlm.nih.gov/PMC6315657/)

84. LIN28A, a sensitive immunohistochemical marker for Embryonal Tumor with Multilayered Rosettes (ETMR), is also positive in a subset of Atypical Teratoid/Rhabdoid Tumor (AT/RT)

Shilpa Rao, R. T. Rajeswarie, T. Chickabasaviah Yasha, Bevinahalli N. Nandeesh, Arimappamagan Arivazhagan, Vani Santosh

Child's Nervous System (2017-07-25) <https://doi.org/ggnpkn>

DOI: [10.1007/s00381-017-3551-6](https://doi.org/10.1007/s00381-017-3551-6) · PMID: [28744687](https://pubmed.ncbi.nlm.nih.gov/28744687/)

85. Childhood Medulloblastoma and Other Central Nervous System Embryonal Tumors Treatment (PDQ®)-Health Professional Version - National Cancer Institute (2008-02-13)

<https://www.cancer.gov/types/brain/hp/child-cns-embryonal-treatment-pdq>

86. DNA Methylation Profiling for Diagnosing Undifferentiated Sarcoma with Capicua Transcriptional Receptor (CIC) Alterations

Evelina Miele, Rita De Vito, Andrea Ciolfi, Lucia Pedace, Ida Russo, Maria Debora De Pasquale, Angela Di Giannatale, Alessandro Crocoli, Biagio De Angelis, Marco Tartaglia, ... Giuseppe Maria Milano

International Journal of Molecular Sciences (2020-03-06) <https://doi.org/ggn7x>

DOI: [10.3390/ijms21051818](https://doi.org/10.3390/ijms21051818) · PMID: [32155762](https://pubmed.ncbi.nlm.nih.gov/32155762/) · PMCID: [PMC7084764](https://pubmed.ncbi.nlm.nih.gov/PMC7084764/)

87. Genomic and Molecular Landscape of DNA Damage Repair Deficiency across The Cancer Genome Atlas

Theo A. Knijnenburg, Linghua Wang, Michael T. Zimmermann, Nyasha Chambwe, Galen F. Gao, Andrew D. Cherniack, Huihui Fan, Hui Shen, Gregory P. Way, Casey S. Greene, ... Armaz Mariamidze

Cell Reports (2018-04) <https://doi.org/gfspsc>

DOI: [10.1016/j.celrep.2018.03.076](https://doi.org/10.1016/j.celrep.2018.03.076) · PMID: [29617664](https://pubmed.ncbi.nlm.nih.gov/29617664/) · PMCID: [PMC5961503](https://pubmed.ncbi.nlm.nih.gov/PMC5961503/)

88. Accelerating Discovery of Functional Mutant Alleles in Cancer

Matthew T. Chang, Tripti Shrestha Bhattacharai, Alison M. Schram, Craig M. Bielski, Mark T. A. Donoghue, Philip Jonsson, Debyani Chakravarty, Sarah Phillips, Cyriac Kandoth, Alexander Penson, ... Barry S. Taylor

Cancer Discovery (2018-02) <https://doi.org/gf9twp>

DOI: [10.1158/2159-8290.cd-17-0321](https://doi.org/10.1158/2159-8290.cd-17-0321) · PMID: [29247016](https://pubmed.ncbi.nlm.nih.gov/29247016/) · PMCID: [PMC5809279](https://pubmed.ncbi.nlm.nih.gov/PMC5809279/)

89. Identifying recurrent mutations in cancer reveals widespread lineage diversity and mutational specificity

Matthew T Chang, Saurabh Asthana, Sizhi Paul Gao, Byron H Lee, Jocelyn S Chapman, Cyriac Kandoth, JianJiong Gao, Nicholas D Soccia, David B Solit, Adam B Olshen, ... Barry S Taylor

Nature Biotechnology (2015-11-30) <https://doi.org/gf7vxp>

DOI: [10.1038/nbt.3391](https://doi.org/10.1038/nbt.3391) · PMID: [26619011](https://pubmed.ncbi.nlm.nih.gov/26619011/) · PMCID: [PMC4744099](https://pubmed.ncbi.nlm.nih.gov/PMC4744099/)

90. The functional domains in p53 family proteins exhibit both common and distinct properties

KL Harms, X Chen

Cell Death & Differentiation (2006-03-17) <https://doi.org/fwgrrt>

DOI: [10.1038/sj.cdd.4401904](https://doi.org/10.1038/sj.cdd.4401904) · PMID: [16543939](#)

91. Gain of function mutations in p53

Dirk Dittmer, Sibani Pati, Gerard Zambetti, Shelley Chu, Angelika K. Teresky, Mary Moore, Cathy Finlay, Arnold J. Levine

Nature Genetics (1993-05) <https://doi.org/crqst7>

DOI: [10.1038/ng0593-42](https://doi.org/10.1038/ng0593-42) · PMID: [8099841](#)

92. Inherited

Tanya Guha, David Malkin

Cold Spring Harbor perspectives in medicine (2017-04-03)

<https://www.ncbi.nlm.nih.gov/pubmed/28270529>

DOI: [10.1101/cshperspect.a026187](https://doi.org/cshperspect.a026187) · PMID: [28270529](#) · PMCID: [PMC5378014](#)

93. The Sequence Alignment/Map format and SAMtools.

Heng Li, Bob Handsaker, Alec Wysoker, Tim Fennell, Jue Ruan, Nils Homer, Gabor Marth, Goncalo Abecasis, Richard Durbin,

Bioinformatics (Oxford, England) (2009-06-08) <https://www.ncbi.nlm.nih.gov/pubmed/19505943>

DOI: [10.1093/bioinformatics/btp352](https://doi.org/10.1093/bioinformatics/btp352) · PMID: [19505943](#) · PMCID: [PMC2723002](#)

94. Inferring Telomerase Enzymatic Activity from Expression Data

Nighat Noureen, Shaofang Wu, Yingli Lyu, Juechen Yang, WK Alfred Yung, Jonathan Gelfond, Xiaojing Wang, Dimpy Koul, Andrew Ludlow, Siyuan Zheng

Cold Spring Harbor Laboratory (2020-05-26) <https://doi.org/ggxfhq>

DOI: <https://doi.org/10.1101/2020.05.21.109249>

95. Inferring Telomerase Enzymatic Activity from Expression Data

Nighat Noureen, Shaofang Wu, Yingli Lyu, Juechen Yang, WK Alfred Yung, Jonathan Gelfond, Xiaojing Wang, Dimpy Koul, Andrew Ludlow, Siyuan Zheng

Cold Spring Harbor Laboratory (2020-05-26) <https://doi.org/ggxfhq>

DOI: [10.1101/2020.05.21.109249](https://doi.org/10.1101/2020.05.21.109249)

96. Telomerase Activity in Germ Cell Cancers and Mature Teratomas

J. Albanell, G. J. Bosl, V. E. Reuter, M. Engelhardt, S. Franco, M. A. S. Moore, E. Dmitrovsky

JNCI Journal of the National Cancer Institute (1999-08-04) <https://doi.org/fb2hjt>

DOI: [10.1093/jnci/91.15.1321](https://doi.org/10.1093/jnci/91.15.1321) · PMID: [10433622](#)

97. TERT promoter mutations are highly recurrent in SHH subgroup medulloblastoma

Marc Remke, Vijay Ramaswamy, John Peacock, David J. H. Shih, Christian Koelsche, Paul A. Northcott, Nadia Hill, Florence M. G. Cavalli, Marcel Kool, Xin Wang, ... Michael D. Taylor

Acta Neuropathologica (2013-10-31) <https://doi.org/f5g9qb>

DOI: [10.1007/s00401-013-1198-2](https://doi.org/10.1007/s00401-013-1198-2) · PMID: [24174164](#) · PMCID: [PMC3830749](#)